

---

**Authors**

J.A. de Gouw, J.B. Gilman, Christopher L. Holloway, B.M. Lerner, M. Graus, J. Peischl, I.B. Pollack, P.R. Veres, C. Warneke, and Please see bottom of page for full list of authors.



## Formaldehyde production from isoprene oxidation across $\text{NO}_x$ regimes

G. M. Wolfe<sup>1,2</sup>, J. Kaiser<sup>3</sup>, T. F. Hanisco<sup>2</sup>, F. N. Keutsch<sup>4</sup>, J. A. de Gouw<sup>5,6</sup>, J. B. Gilman<sup>5,6</sup>, M. Graus<sup>5,6,a</sup>, C. D. Hatch<sup>7</sup>, J. Holloway<sup>5,6</sup>, L. W. Horowitz<sup>8</sup>, B. H. Lee<sup>9</sup>, B. M. Lerner<sup>5,6</sup>, F. Lopez-Hilfiker<sup>9,b</sup>, J. Mao<sup>8,11</sup>, M. R. Marvin<sup>10</sup>, J. Peischl<sup>5,6</sup>, I. B. Pollack<sup>5,6</sup>, J. M. Roberts<sup>6</sup>, T. B. Ryerson<sup>6</sup>, J. A. Thornton<sup>9</sup>, P. R. Veres<sup>5,6</sup>, and C. Warneke<sup>5,6</sup>

<sup>1</sup>Joint Center for Earth Systems Technology, University of Maryland Baltimore County, Baltimore, MD, USA

<sup>2</sup>Atmospheric Chemistry and Dynamics Laboratory, NASA Goddard Space Flight Center, Greenbelt, MD, USA

<sup>3</sup>Department of Chemistry, University of Wisconsin–Madison, Madison, WI, USA

<sup>4</sup>School of Engineering and Applied Sciences and Department of Chemistry and Chemical Biology, Harvard University, Cambridge, MA, USA

<sup>5</sup>Cooperative Institute for Research in Environmental Sciences, University of Colorado Boulder, Boulder, CO, USA

<sup>6</sup>Chemical Sciences Division, NOAA Earth System Research Laboratory, Boulder, CO, USA

<sup>7</sup>Department of Chemistry, Hendrix College, Conway, AR, USA

<sup>8</sup>NOAA Geophysical Fluid Dynamics Laboratory, Princeton, NJ, USA

<sup>9</sup>Department of Atmospheric Sciences, University of Washington, Seattle, WA, USA

<sup>10</sup>Department of Chemistry, University of Maryland, College Park, MD, USA

<sup>11</sup>Program in Atmospheric and Oceanic Sciences, Princeton University, Princeton, NJ, USA

<sup>a</sup>now at: Institute of Atmospheric and Cryospheric Sciences, Innsbruck University, Innsbruck, Austria

<sup>b</sup>now at: Laboratory of Atmospheric Chemistry, Paul Scherrer Institut, 5232 Villigen, Switzerland

Correspondence to: G. M. Wolfe (glenn.m.wolfe@nasa.gov)

Received: 28 October 2015 – Published in Atmos. Chem. Phys. Discuss.: 11 November 2015

Revised: 2 February 2016 – Accepted: 20 February 2016 – Published: 2 March 2016

**Abstract.** The chemical link between isoprene and formaldehyde (HCHO) is a strong, nonlinear function of  $\text{NO}_x$  (i.e.,  $\text{NO} + \text{NO}_2$ ). This relationship is a linchpin for top-down isoprene emission inventory verification from orbital HCHO column observations. It is also a benchmark for overall photochemical mechanism performance with regard to VOC oxidation. Using a comprehensive suite of airborne in situ observations over the southeast US, we quantify HCHO production across the urban–rural spectrum. Analysis of isoprene and its major first-generation oxidation products allows us to define both a “prompt” yield of HCHO (molecules of HCHO produced per molecule of freshly emitted isoprene) and the background HCHO mixing ratio (from oxidation of longer-lived hydrocarbons). Over the range of observed  $\text{NO}_x$  values (roughly 0.1–2 ppbv), the prompt yield increases by a factor of 3 (from 0.3 to 0.9 ppbv ppbv<sup>-1</sup>), while background HCHO increases by a factor of 2 (from 1.6 to 3.3 ppbv). We apply the same method to evaluate the performance of both a

global chemical transport model (AM3) and a measurement-constrained 0-D steady-state box model. Both models reproduce the  $\text{NO}_x$  dependence of the prompt HCHO yield, illustrating that models with updated isoprene oxidation mechanisms can adequately capture the link between HCHO and recent isoprene emissions. On the other hand, both models underestimate background HCHO mixing ratios, suggesting missing HCHO precursors, inadequate representation of later-generation isoprene degradation and/or underestimated hydroxyl radical concentrations. Detailed process rates from the box model simulation demonstrate a 3-fold increase in HCHO production across the range of observed  $\text{NO}_x$  values, driven by a 100 % increase in OH and a 40 % increase in branching of organic peroxy radical reactions to produce HCHO.

## 1 Introduction

Formaldehyde (HCHO) is a ubiquitous byproduct of volatile organic compound (VOC) oxidation. While methane is the principal HCHO precursor in remote regions, larger VOC are the main source over continents. HCHO is also directly emitted via biomass burning (Lee et al., 1997), fossil fuel combustion (Luecken et al., 2012), natural gas flaring (Knighton et al., 2012), ethanol refining (de Gouw et al., 2015), and possibly vegetation (DiGangi et al., 2011) and agricultural activity (Kaiser et al., 2015a), but chemical production dominates the global budget (Fortems-Cheiney et al., 2012). Photolysis and reaction with OH destroy HCHO with a characteristic lifetime of several hours during midday, implying that the HCHO abundance reflects recent VOC oxidation.

Globally, isoprene is the main precursor of near-surface HCHO. A highly reactive diene emitted by vegetation, isoprene comprises roughly one-third of all non-methane VOC emissions (Guenther et al., 2012). Oxidation of isoprene in the presence of nitrogen oxides (NO<sub>x</sub> = NO + NO<sub>2</sub>) stimulates the production of ozone (Trainer et al., 1987) and organic aerosol precursors (Xu et al., 2015), impacting air quality and climate in many continental regions. Biogenic emission inventories struggle to accurately represent the spatiotemporal variability of isoprene emissions, with model–measurement discrepancies and differences among emission inventories approaching a factor of 2 or more (Carlton and Baker, 2011; Warneke et al., 2010). Such differences directly impact predicted ozone and aerosol distributions (Hogrefe et al., 2011).

Numerous studies have applied satellite-based HCHO column observations as a top-down constraint on isoprene emissions (see Kefauver et al., 2014, for a review). Typically, a chemical transport model is employed both to supply a priori HCHO vertical distributions for satellite retrievals (González Abad et al., 2015) and to relate HCHO column concentrations to isoprene emission strength. Earlier studies utilized linear steady-state relationships (Palmer et al., 2003), while recent computational advances have permitted full inversions that more fully account for transport, multiple sources and varying chemical regimes (Fortems-Cheiney et al., 2012). Such techniques have informed isoprene emission inventories in North America (Abbot et al., 2003; Millet et al., 2006, 2008; Palmer et al., 2003, 2006), South America (Barkley et al., 2008, 2013), Europe (Curci et al., 2010; Dufour et al., 2009), Africa (Marais et al., 2012), Asia (Fu et al., 2007; Stavrakou et al., 2014), and globally (Fortems-Cheiney et al., 2012; Shim et al., 2005; Stavrakou et al., 2009). Future geostationary observations, such as the NASA Tropospheric Emissions: Monitoring of Pollution (TEMPO, <http://science.nasa.gov/missions/tempo/>) mission, will permit an even more detailed investigation of the spatial and temporal variability of isoprene emissions and other VOC sources.

Chemistry dictates the relationship between HCHO columns and underlying isoprene emissions. Many of the

above-listed studies apply 0-D box model calculations to evaluate the yield of HCHO from isoprene as a function of oxidation time, NO<sub>x</sub> regime and chemical mechanism. In all cases, it is found that NO<sub>x</sub> enhances both the production rate and ultimate yield of HCHO. Slower production at lower NO<sub>x</sub> can lead to “smearing”, whereby HCHO production is displaced relative to the isoprene source. Palmer et al. (2003) define a characteristic smearing length scale, which can range from 10 to 100 km or more. Furthermore, accumulation of oxygenated VOC over multiple generations of isoprene degradation can contribute to substantial background HCHO production, which is not directly linked with fresh isoprene emissions. Long-lived primary anthropogenic or biogenic emissions, like methane and methanol, can also contribute to this background. Background column concentrations are typically on the order of  $5 \times 10^{15} \text{ cm}^{-2}$ , equal to 20% or more of the isoprene-driven HCHO column enhancement (Barkley et al., 2013; Millet et al., 2006). A wave of recent theoretical (Peeters et al., 1999, 2014; Peeters and Müller, 2010), laboratory (Crouse et al., 2011, 2012; Paulot et al., 2009a, b) and field (Mao et al., 2012) research has highlighted shortcomings in low-NO<sub>x</sub> isoprene oxidation schemes. Such issues translate directly into top-down emission estimates; for example, Marais et al. (2012) report an uncertainty of 40% in satellite-derived African isoprene emissions at high NO<sub>x</sub> and 40–90% at low NO<sub>x</sub>. Coarse resolution of averaged satellite observations and model simulations (typically  $1^\circ \times 1^\circ$  or more) has partly mitigated these problems in prior work, as variability in NO<sub>x</sub>-dependent smearing and background production is averaged out. A more careful treatment will be needed to harness the enhanced resolution of near-future orbital observations (e.g.,  $8 \times 4.5 \text{ km}^2$  for TEMPO), especially since these measurements will include diurnal variability.

Here, we use a comprehensive set of in situ observations to quantify the impact of NO<sub>x</sub> on the isoprene–HCHO chemical link. Using isoprene and its unique first-generation products, we segregate HCHO into two categories. The first, defined as “prompt” HCHO, is produced from fresh isoprene emissions (on a timescale of less than a day) and retains the signature of isoprene emission source strength. The second category is “background” HCHO stemming from oxidation of longer-lived isoprene oxidation products and other VOC. We examine the NO<sub>x</sub> dependence of both quantities. Applying the same method to 0-D and global model simulations, we evaluate the ability of current chemical mechanisms to replicate the observed trends. Box model results are also used to elucidate the mechanistic underpinnings of the NO<sub>x</sub> influence on HCHO production.

## 2 SENEX observations

The Southeast Nexus (SENEX) mission was an airborne campaign designed to examine the interaction of natural and

anthropogenic emissions (Warneke et al., 2016). During June and July of 2013, the NOAA WP-3D aircraft logged about 120 flight hours over 20 research flights in a range of environments throughout the southeast United States, including urban centers, power plant plumes, natural gas extraction regions, agricultural areas and forests. The payload included a suite of gas- and particle-phase instrumentation. Here we utilize observations of HCHO, isoprene, methyl vinyl ketone (MVK), methacrolein (MACR), NO and NO<sub>2</sub>. HCHO was measured at 1 Hz by the NASA In Situ Airborne Formaldehyde (ISAF) instrument, which utilizes the laser-induced fluorescence technique and has an accuracy of  $\pm 10\%$  (Cazorla et al., 2015). Isoprene, MVK and MACR were measured by both a quadrupole proton transfer reaction mass spectrometer (PTR-MS) and the NOAA improved whole-air sampler (iWAS) with offline gas chromatography. The PTR-MS (de Gouw and Warneke, 2007) has a stated accuracy of 20% and sequentially sampled masses for isoprene ( $m/z + 69$ ) and the sum of MVK and MACR ( $m/z + 71$ ) for 1 s each with a duty cycle of 14 s. The iWAS (Lerner et al., 2016) collected 72 canister samples each flight, which were analyzed offline with gas chromatography–mass spectrometry 3–4 days post-flight. iWAS measurement uncertainty is 20% for speciated MVK and MACR and 27% for isoprene. NO and NO<sub>2</sub> were measured at 1 Hz via chemiluminescence coupled with a photolytic NO<sub>2</sub> converter (Pollack et al., 2010; Ryerson et al., 1999) with an accuracy of 5%. Data are filtered to include only daytime boundary-layer conditions (solar zenith angle  $< 60^\circ$ , radar altitude  $< 1$  km). Influence from biomass burning (acetonitrile  $> 210$  pptv and CO  $> 300$  ppbv) is also removed. This procedure, along with the disjunct nature of the PTR-MS measurement, excludes 50% of all fast (1 Hz) data. After accounting for data gaps, we retain 8435 1 Hz data points and 81 iWAS samples.

Measurements of MVK and MACR may include a positive bias from conversion of isoprene hydroxyhydroperoxides (ISOPOOH) on hot metal surfaces in the sampling system (Liu et al., 2013; Rivera-Rios et al., 2014). ISOPOOH mixing ratios up to 2 ppbv were observed during SENEX by the University of Washington iodide-adduct high-resolution time-of-flight chemical ionization mass spectrometer. Neither the NOAA PTR-MS nor the iWAS has been tested for this interference with an ISOPOOH standard; thus we cannot definitively rule out such artifacts or develop a correction factor. To our knowledge, it is not yet clear how the putative interference depends on instrument configuration (flow rates, electric fields, etc.). Thus, caution is warranted when comparing the SENEX systems to similar, but not identical, instruments. Theoretically, this mechanism could give rise to an analogous artifact in HCHO observations. Recent laboratory tests, however, indicate that the ISOPOOH-to-HCHO conversion efficiency in ISAF is less than 5% (St. Clair et al., 2016).

We cannot unambiguously quantify the ISOPOOH artifact using observations alone, but we can gain some insight from

comparing PTR-MS and iWAS data. On average, iWAS observations of MVK+MACR are  $\sim 40\%$  higher than those from the PTR-MS (Figs. S1 and S2 in the Supplement), suggesting a systematic bias in one or both measurements. Both instruments were calibrated using the same gas standards, and the two techniques agree well for other species such as isoprene (Lerner et al., 2016; Warneke et al., 2016), so a calibration error is unlikely. Production of oxygenated VOC in ambient air samples collected and aged in stainless steel canisters cannot be ruled out. Enhancements in MVK and MACR (above the 20% uncertainty) have been observed in canisters after aging over  $\sim 11$  days (Lerner et al., 2016), though this is significantly longer than typical turn-around times for SENEX. To evaluate the potential for ISOPOOH conversion to explain this discrepancy, we plot the ratio and difference of the PTR-MS and iWAS measurements as a function of ISOPOOH in Fig. S2 in the Supplement. While the ratio is essentially constant (iWAS/PTR-MS  $\sim 1.43$ ), the absolute difference exhibits a strong positive correlation with ISOPOOH ( $r^2 = 0.43$ ). The slope of this relationship implies that a conversion of 50% of ISOPOOH to MVK and/or MACR in the iWAS system would explain the difference in the two measurements. Correcting total iWAS MVK+MACR for such an artifact reduces the slope of the iWAS–PTR-MS correlation from 1.48 to 1.24 (Fig. S1B in the Supplement), bringing agreement to within combined measurement uncertainties. In practice, we cannot apply such a correction to the speciated iWAS observations as the conversion efficiency may be different for each isomer. This result does not exclude the possibility of an artifact in the PTR-MS measurement, though it does suggest an upper limit ISOPOOH conversion efficiency of 50% for the PTR-MS (which would imply a conversion of 100% for the iWAS). The analysis presented in Sects. 3 and 4 primarily relies on PTR-MS data due to its greater temporal coverage. Our key conclusions are not impacted by a 50% ISOPOOH correction to the PTR-MS data, and thus we use the data without correction.

SENEX sampled a wide spectrum of chemical regimes (Fig. 1). For the daytime boundary-layer observations presented here, maximum 1 Hz isoprene and NO mixing ratios respectively reach 8.1 and 95 ppbv, while minima are less than a few pptv. The distributions of both isoprene and NO observations are approximately log-normal (top and right panels of Fig. 1), peaking at 1.5 ppbv and 50 pptv, respectively. Though these distributions may be biased towards areas of urban influence, the range of environments encountered during SENEX is representative of the southeast US summertime boundary layer. The long tail at the low end of the isoprene distribution is mostly associated with regions lacking significant tree cover where isoprene emissions are lower, notably Illinois and Indiana. The NO distribution spans 4 orders of magnitude ( $< 10$  to  $\sim 10^4$  pptv), over which radical chemistry changes markedly. At NO mixing ratios of a few hundred pptv or more, organic peroxy radicals (RO<sub>2</sub>)

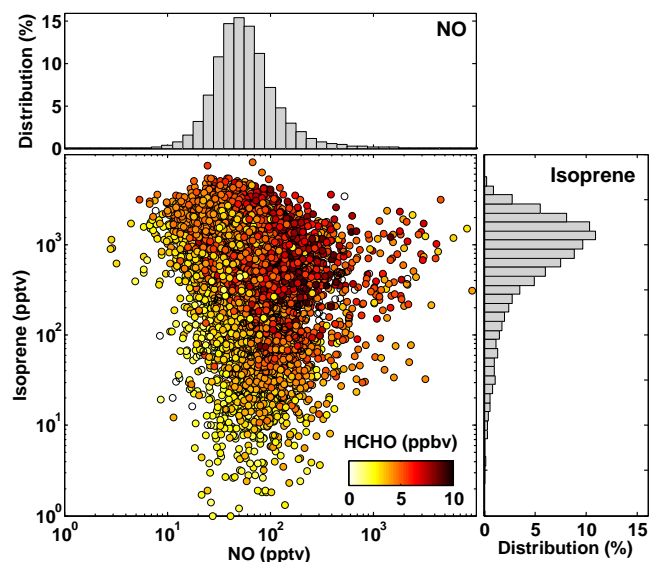


**Figure 1.** Covariation of isoprene, NO and HCHO mixing ratios in the summertime southeast US. Data are limited to daytime boundary-layer observations. Histograms show the corresponding NO and isoprene distributions.

react mostly with NO. At low NO (tens of pptv or less), reaction with HO<sub>2</sub>, other RO<sub>2</sub> and isomerization dominate the RO<sub>2</sub> fate (Fig. S6 in the Supplement). The bulk of the NO distribution lies in a transition region for radical chemistry, making this data set ideal for probing the anthropogenic influence on biogenic VOC oxidation.

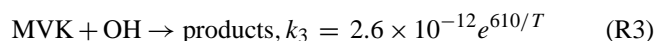
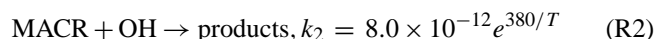
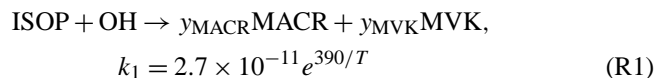
HCHO mixing ratios (color shading in Fig. 1) range from 0.8 to 14 ppbv with a mean of 4.3 ppbv. HCHO is most abundant in regions where both isoprene and NO<sub>x</sub> are elevated. High NO<sub>x</sub> is often accompanied by increased concentrations of anthropogenic VOC; however, constrained box model calculations demonstrate that isoprene is the dominant HCHO precursor even in these cases (Sect. 5). Thus, changes in radical cycling and partitioning (and not covariance of NO<sub>x</sub> and anthropogenic VOC) drive the observed NO<sub>x</sub> dependence of HCHO abundance.

### 3 Linking observed and emitted isoprene

The isoprene photochemical cascade is a multi-step process. Isoprene oxidation is initiated via reaction with the hydroxyl radical (OH), ozone, or the nitrate radical (NO<sub>3</sub>). In the southeast US, typical daytime levels for OH, ozone and NO<sub>3</sub> are  $4 \times 10^6 \text{ cm}^{-3}$ , 50 ppbv and 0.1 pptv, respectively (OH and NO<sub>3</sub> are estimated from median box model output; see Sect. 5). The corresponding isoprene lifetimes at 298 K are 0.7, 17 and 160 h, respectively. Thus, reaction with OH typically constitutes 95 % or more of the total daytime isoprene sink in this environment. Addition of OH and reaction with O<sub>2</sub> generates one of several isoprene hydroperoxy radicals

(ISOPO<sub>2</sub>). ISOPO<sub>2</sub> isomers interconvert rapidly due to reversible O<sub>2</sub> addition (Peeters et al., 2009) but are eventually destroyed via reaction with NO, hydroperoxy radical (HO<sub>2</sub>), other organic peroxy radicals (RO<sub>2</sub>) or isomerization. Most branches have the potential to produce HCHO, with varying yields. The laboratory-derived first-generation HCHO yield from the NO pathway is  $\sim 0.6$  (Atkinson and Arey, 2003), though this value may be less representative of the real atmosphere due to the very high isoprene concentrations (and very short RO<sub>2</sub> lifetimes) in early chamber experiments. The first-generation yield from the HO<sub>2</sub> pathway is  $\sim 0.06$  (Liu et al., 2013). Isomerization chemistry is less well understood; the 1,5-H shift is believed to produce HCHO with a unity yield, while the much faster 1,6-H shift should not produce any HCHO (da Silva et al., 2010; Fuchs et al., 2013; Peeters et al., 2009, 2014; Peeters and Müller, 2010). Regardless of the specific pathway, MVK or MACR are always co-produced with HCHO in the first generation. HCHO is also generated in subsequent chemistry, but on a longer timescale and from a much larger suite of precursors. For example, the OH lifetimes of MACR and MVK are respectively 3.5 and 5 times longer than that of isoprene. HCHO, MVK and MACR are also high-yield products of isoprene ozonolysis (Atkinson and Arey, 2003), but as noted above this reaction is relatively slow. Nighttime oxidation of isoprene by NO<sub>3</sub> radical is also likely a negligible source of these carbonyls (Brown et al., 2009). Yields are small (Atkinson and Arey, 2003; Kwok et al., 1996), and the lifetimes of MVK, MACR and HCHO are sufficiently short that any nighttime production should not influence the midday observations considered here.

Boundary layer composition reflects a mixture of emissions with various degrees of photochemical processing. To isolate the impact of “fresh” isoprene emissions, we exploit the relatively simple chemistry of MVK and MACR, which are produced via isoprene (ISOP) oxidation and lost primarily via reaction with OH.



Rate constants ( $k$ ) are taken from the IUPAC database (Atkinson et al., 2006). These reactions form the basis for a photochemical clock of isoprene oxidation (de Gouw et al., 2005; Roberts et al., 2006; Stroud et al., 2001). Integration of the kinetic equations for this system shows that the product/parent ratios are a function of the rate constants, yield ( $y$ ), reaction time ( $t$ ) and mean OH concentration. In the case of MACR, for example,

$$\frac{[\text{MACR}]}{[\text{ISOP}]} = \frac{y_{\text{MACR}}k_1}{k_2 - k_1} (1 - \exp((k_1 - k_2)[\text{OH}]t)). \quad (1)$$

An analogous expression holds for MVK. As noted by Stroud et al. (2001), this “sequential reaction model” is purely chem-

ical and does not account for the effects of mixing and transport. Indeed, this analysis relates daughter/parent ratios to an “average” photochemical age, when in fact there is a broad distribution of ages in any mixed air mass. We also implicitly assume that direct emissions (Fares et al., 2015) and deposition (Karl et al., 2010) of MVK and MACR do not significantly influence the budget of these compounds.

Two potential issues arise when applying this model to the real atmosphere. First, the yields of MVK and MACR are dependent on ISOPO<sub>2</sub> branching and are thus a nonlinear function of NO<sub>x</sub>. Previous applications of this method (de Gouw et al., 2005; Roberts et al., 2006; Stroud et al., 2001) have assumed lab-derived high-NO<sub>x</sub> yields of 0.33 and 0.23 for MVK and MACR, respectively (Atkinson and Arey, 2003), but this may not be appropriate in the present case; furthermore, these yields are not fully consistent with current chemical mechanisms. Given the wide range of conditions sampled, we explicitly account for NO<sub>x</sub>-dependent yields for MVK and MACR. For this purpose, we conducted a series of pseudo-chamber simulations using a box model driven by the Master Chemical Mechanism (MCM) v3.3.1 (Jenkin et al., 2015). As described in the Supplement, model setup mimics typical daytime conditions in the southeast US (Fig. S3B in the Supplement), and yields are derived using a standard procedure. Resulting yield curves (Fig. S3A in the Supplement) are then interpolated to observed NO mixing ratios. Second, the photochemical age (*t*) implied by any observed daughter/parent ratio depends on the concentration of OH, which was not measured and varies as an air mass ages. Rather than assume a single “typical” value for OH, we express photochemical age in terms of “exposure”, defined here as the product of OH concentration and reaction time averaged over the photochemical lifetime of an air mass.

Figure 2 compares the observed relationship of iWAS MVK/isoprene and MACR/isoprene ratios against theoretical trends predicted by the sequential reaction model. Theoretical ratios are calculated at fixed exposures of 2, 4, 8, 12 and 16 × 10<sup>6</sup> OH cm<sup>-3</sup> h using model-derived yields for the 5th/95th percentiles of the observed NO distribution (NO = 20/200 pptv,  $y_{\text{MVK}} = 0.18/0.38$ ,  $y_{\text{MACR}} = 0.11/0.20$ ). Observed ratios of MVK/isoprene versus MACR/isoprene exhibit a tight linear correlation. Higher ratios are often associated with higher NO<sub>x</sub>, likely reflecting enhanced OH and higher product yields in these air masses. Far downwind from isoprene and NO<sub>x</sub> source regions, we would expect to see higher MVK/isoprene and MACR/isoprene ratios associated with lower NO<sub>x</sub> due to removal of the latter. The theoretical slope agrees well with observations, indicating exposures of 1–16 × 10<sup>6</sup> OH cm<sup>-3</sup> h. For a typical daytime OH concentration of 4 × 10<sup>6</sup> cm<sup>-3</sup>, this corresponds to processing times of 0.25–4 h.

The assumed MVK and MACR yields dictate the correspondence between daughter/parent ratios and exposure. For example, a MACR/isoprene ratio of 1 would be consistent with an exposure of 7.9 × 10<sup>6</sup>

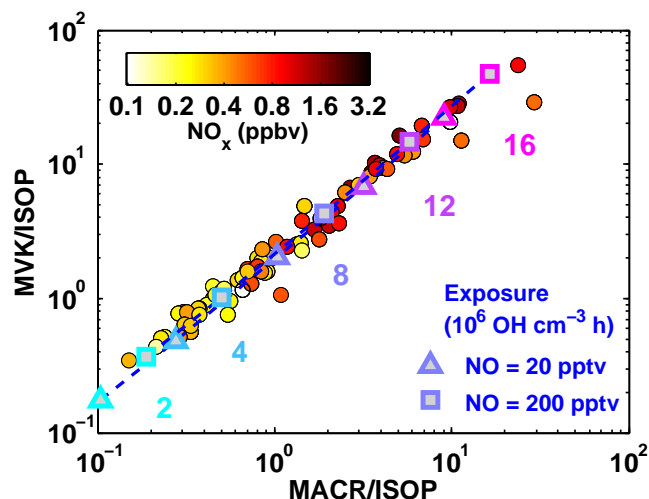


**Figure 2.** A photochemical clock of isoprene oxidation defined by the progression of daughter/parent ratios. Solid circles show the observed ratios calculated from iWAS observations, colored by NO<sub>x</sub>. Blue/purple symbols, dashed lines, and text indicate the theoretical exposures (the product of OH concentration and time) corresponding to any given daughter–parent relationship. Theoretical values are calculated at 298 K using MVK and MACR yields for NO values of 20 pptv (triangles) and 200 pptv (squares).

OH cm<sup>-3</sup> h at NO = 20 pptv versus 6.0 × 10<sup>6</sup> OH cm<sup>-3</sup> h at NO = 200 pptv. Thus, for any given daughter/parent ratio, a higher assumed yield gives a smaller derived exposure. The ratio of  $y_{\text{MVK}}$  to  $y_{\text{MACR}}$  determines the location of the theoretical line, and the excellent agreement of this relationship with observations in Fig. 2 indicates that MCM v3.3.1 accurately represents the branching ratios for MVK and MACR production within the sampled NO<sub>x</sub> range.

We can effectively reverse this photochemical clock to derive a proxy for the total isoprene emissions that have been released into the sample air masses (de Gouw et al., 2005). First, we calculate OH exposures from observed daughter/parent ratios by inverting Eq. (1). To perform this calculation with PTR-MS data (which have far greater coverage than the iWAS), we partition the measured sum between MVK and MACR using MVK/MACR ratios from steady-state box model calculations (Sect. 5). Modeled MVK/MACR ratios (with an output interval of 1 min) are linearly interpolated to the 14 s observational time base. The MVK/MACR ratio does not vary dramatically (mean ± 1σ: 2.3 ± 0.2), and using a constant ratio instead alters exposures by less than 4%. Calculated exposures range from 1 to 20 × 10<sup>6</sup> OH cm<sup>-3</sup> h (Fig. S4A in the Supplement). Exposures derived from MACR are 6% lower than those from MVK on average, and we use the mean of these two values. Next, an “initial” isoprene mixing ratio, ISOP<sub>0</sub>, is estimated via reverse integration of isoprene’s first-order loss rate:

$$[\text{ISOP}]_0 = [\text{ISOP}] \exp(k_1 [\text{OH}] t). \quad (2)$$

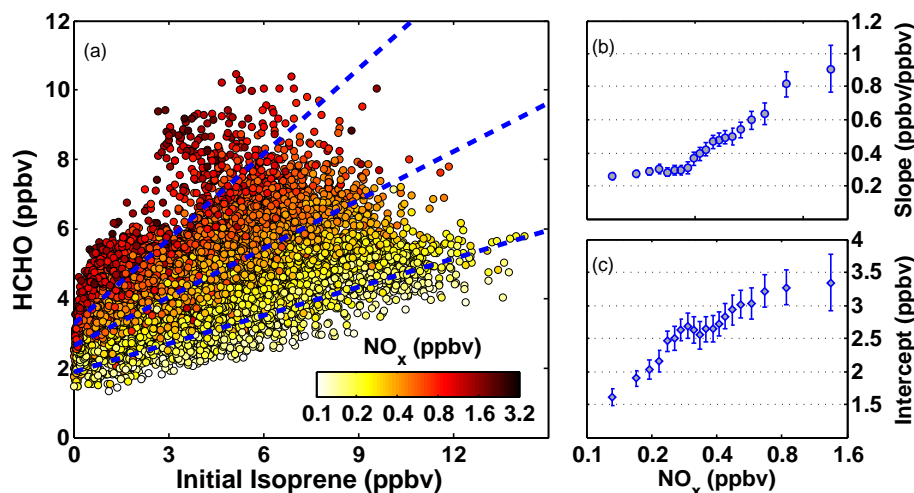


**Figure 3.** (a)  $\text{NO}_x$  modulates the relationship between observed HCHO and calculated initial isoprene mixing ratios. Symbols denote all 1 Hz data. Dashed lines illustrate representative major-axis fits of  $\text{NO}_x$ -grouped subsets at mean  $\text{NO}_x$  values of 170, 380 and 810 pptv (see text for details of fitting procedure). The slope (b) and intercept (c) of these fits are the prompt HCHO yield and background HCHO mixing ratio, respectively. Error bars in (b) and (c) are  $3\sigma$  fitting uncertainties.

$\text{ISOP}_0$  represents the amount of isoprene that an air parcel would have to start with to generate the amount of isoprene, MVK and MACR observed. Thus, it is an observationally constrained surrogate for isoprene emission strength (modulated to some degree by boundary-layer height, as it is a volume-based quantity).  $\text{ISOP}_0$  mixing ratios are typically 2–20 times higher than observed isoprene (Fig. S4B in the Supplement).

#### 4 The yield of HCHO from isoprene

The definition of “yield” can vary with context and requires careful consideration when quantifying chemical relationships. In a mechanistic sense, the “first-generation yield” refers to the amount of HCHO produced per unit isoprene consumed in the first stage of oxidation. This is analogous to the yields of MVK and MACR used in the above calculation of initial isoprene. The model-derived first-generation HCHO yield from isoprene varies by more than a factor of 2 over the range of chemical environments encountered during SENEX (Fig. S3 in the Supplement). An alternative definition is that of the “total yield” (sometimes referred to as the “molar yield”; e.g., Millet et al., 2006), a time-dependent quantity that describes the total amount of HCHO produced over multiple generations of oxidation. The total yield is typically derived from model simulations and used to relate satellite HCHO column observations to isoprene emissions (Marais et al., 2012; Millet et al., 2006). Earlier studies acknowledged the  $\text{NO}_x$  dependence of the total yield (Millet et al., 2006; Palmer et al., 2003), and more recent work has attempted to account for this dependence using  $\text{NO}_2$  column observations (Marais et al., 2012). Here, we define the

“prompt yield” as the change in observed HCHO per unit change in  $\text{ISOP}_0$  ( $\Delta\text{HCHO} / \Delta\text{ISOP}_0$ ). This is not the same as the first-generation yield, since the prompt yield can include HCHO production and loss over several hours (depending on the photochemical exposure of an air mass). Nor is it the same as the total yield, which inherently does not account for HCHO loss as an air mass ages. The prompt yield is effectively a quantity that relates isoprene emission strength to observed HCHO abundance. As we will demonstrate, this quantity is well suited for segregating the various drivers of HCHO and for benchmarking model performance.

Figure 3a shows the relationship between calculated  $\text{ISOP}_0$  and observed HCHO. The overall correlation is linear with a striking  $\text{NO}_x$  gradient. To quantify this  $\text{NO}_x$  dependence, we sort the data by  $\log(\text{NO}_x)$ , group it into 20 bins such that each bin contains the same number of points ( $N = 416$ ), and perform a major-axis linear fit of HCHO versus  $\text{ISOP}_0$  for each bin. Individual fits give  $r^2$  values of 0.6–0.8, except for the highest  $\text{NO}_x$  bin ( $r^2 = 0.48$ ) that contains some heavily polluted air masses, such as downwind from power plants. Very fresh power plant plumes, defined as  $\log(\text{NO}_x)$  values exceeding a mean  $+3\sigma$  threshold, are removed prior to this procedure to avoid skewing the highest  $\text{NO}_x$  bin. Results are independent of the number of bins chosen or time resolution (e.g., 1 s versus 1 min data).

The HCHO– $\text{ISOP}_0$  slope (Fig. 3b) represents the prompt yield. This yield varies by a factor of 3 over the range of observed  $\text{NO}_x$ , from 0.3 ppbv ppbv $^{-1}$  for  $\text{NO}_x$  mixing ratios of a few hundred pptv to 0.9 ppbv ppbv $^{-1}$  at  $\text{NO}_x > 1$  ppbv. At low  $\text{NO}_x$ , the prompt yield is comparable to the MCM-predicted direct first-generation yield of HCHO (0.25–0.4 ppbv ppbv $^{-1}$  at  $\text{NO} = 10$ –40 pptv, Fig. S3 in the

Supplement), while at high NO<sub>x</sub> it is somewhat higher than the predicted first-generation yield (0.75 ppbv ppbv<sup>-1</sup> at NO = 1000 pptv). This likely reflects the inclusion of more than one generation of HCHO production at higher NO<sub>x</sub>, where oxidation is more rapid (median exposures increase by 38 % over the range of observed NO<sub>x</sub> values). Most of this portion of the HCHO budget, however, stems from first-generation production.

The intercept (Fig. 3c) represents the abundance of “background” HCHO. This portion of the HCHO budget stems mainly from air that either has not encountered strong isoprene emissions or is so aged that most of the isoprene has reacted away and can no longer be linked to a specific source region. Some of this background may also stem from oxidation of long-lived primary emissions like methane or methanol. Box model calculations (Sect. 5) indicate average HCHO budget contributions of  $0.3 \pm 0.2$  and  $0.2 \pm 0.1$  ppbv from methane and methanol, respectively. Background HCHO also exhibits a marked NO<sub>x</sub> dependence, increasing from 1.6 to 3.3 ppbv over the observed NO<sub>x</sub> range. As with the prompt yield, we expect such behavior since NO<sub>x</sub> regulates the fate of all organic peroxy radicals (see Sect. 6). Assuming a 1 km mixed layer depth (Wagner et al., 2015), the corresponding HCHO column density for this background is  $4\text{--}8 \times 10^{15} \text{ cm}^{-2}$ . This is comparable to the background reported by previous investigations of satellite-derived HCHO columns (Barkley et al., 2013; Millet et al., 2006). None of these studies explicitly account for the NO<sub>x</sub> dependence of the background, though it can represent a substantial fraction of the total HCHO column – maximum summertime HCHO columns over the southeast US are  $\sim 25 \times 10^{15} \text{ cm}^{-2}$  (Millet et al., 2008). Given the strong NO<sub>x</sub> dependence of both prompt and background HCHO, grouping HCHO column observations by NO<sub>x</sub> (e.g., using simultaneous observations of NO<sub>2</sub> columns (Marais et al., 2012) or model-derived NO<sub>x</sub>) and performing an analysis similar to that described here could provide a robust means of accounting for these influences.

## 5 Model evaluation

Next, we compare the observed HCHO–ISOP<sub>0</sub> relationship to results from a global chemical-transport model and a 0-D box model. Our goals are to both illustrate the utility of this analysis and evaluate model performance. By going beyond a simple comparison of modeled and measured mixing ratios, we can more accurately pinpoint potential shortcomings in model chemistry.

The GFDL AM3 model is an atmospheric general circulation model with interactive chemistry (Donner et al., 2011), including recent updates to the representation of isoprene degradation (Mao et al., 2013; Naik et al., 2013). Model simulations were carried out at 50 km × 50 km resolution with horizontal winds nudged to NCEP GFS analyses and sam-

pled along the SENEX flight tracks at a time resolution of 1 min. Further details are available elsewhere (Li et al., 2016).

The University of Washington Chemical Box Model (UWCM v2.2) is a versatile zero-dimensional framework for simulating various chemical systems, including lab chamber experiments (Wolfe et al., 2012) and observations from ground (Kim et al., 2013, 2015; Wolfe et al., 2014) and airborne (Marvin et al., 2016) platforms. Multiple chemical mechanisms are available within UWCM; here we used the latest version of the Master Chemical Mechanism (MCM v3.3.1; Jenkin et al., 2015). UWCM was constrained with 1 min average observations of isoprene, NO<sub>2</sub>, ozone, CO, PAN, methane, methanol and meteorology and assumed clear-sky conditions for photolysis frequencies. The chemical system was integrated forward in time to diel steady state (total integration time of 3 days) for each set of measurements. This setup inherently assumes that the atmosphere is in chemical steady state – that is, that production and loss of HCHO, MVK, MACR and other species are roughly balanced. This assumption is rarely strictly true and may fail for highly aged air masses (where isoprene is depleted) or when close to strong local emissions. Nonetheless, it is a fair approximation for the daytime well-mixed boundary-layer observations that prevailed during SENEX. Monoterpenes and anthropogenic VOC are excluded from the simulation since observations of these species (from the iWAS) are relatively sparse. Separate sensitivity simulations utilizing the iWAS data suggest that observed monoterpenes and anthropogenic VOC (a subset of alkanes, alkenes and aromatics) increase modeled HCHO by  $1 \pm 2$  and  $2 \pm 3$  %, respectively. A more detailed evaluation of box model performance is forthcoming (Marvin et al., 2016).

Outputs from both models are filtered for daytime, boundary-layer, non-biomass-burning points using the same criteria as that for observations (Sect. 2). Both models adequately reproduce observed HCHO mixing ratios (Fig. S5 in the Supplement). We perform the same analyses as described above to derive model prompt yield and background HCHO. Because of the reduced time resolution, we group results into 10 NO<sub>x</sub> bins, instead of 20, before fitting. For AM3, this results in 172 points per bin and typical  $r^2$  values of 0.4–0.8. For UWCM, there are 134 points per bin and all  $r^2$  values are  $> 0.86$ .

Both AM3 and UWCM reproduce the observed NO<sub>x</sub> dependence of the prompt yield (Fig. 4a). AM3 agrees well with observations in both magnitude and trend, though with some scatter at mid-NO<sub>x</sub> levels. UWCM tends to be slightly low throughout most of the NO<sub>x</sub> range, which may reflect an issue with the mechanism (discussed below) or an inherent shortcoming of the steady-state assumption. Regardless of minor differences, these results suggest that both models provide excellent representation of early generation isoprene oxidation across NO<sub>x</sub> regimes.

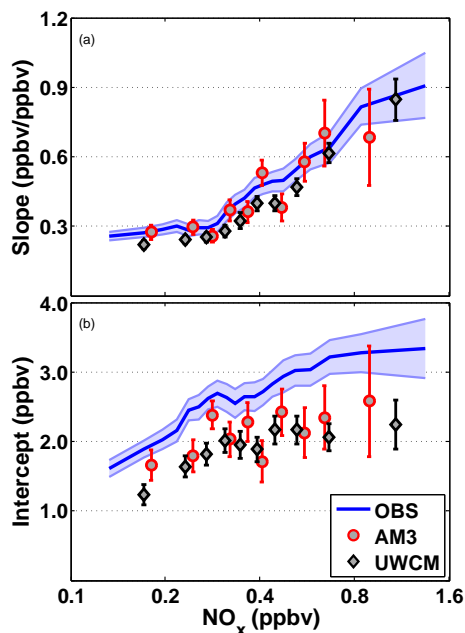


**Figure 4.** Comparison of observed and model-derived relationships between HCHO and initial isoprene versus  $\text{NO}_x$ . Slopes (a) and intercepts (b) are calculated as described in the text. The observed values (blue line with shading) are the same as those shown in Fig. 3b–c. Symbols represent fit results for the global AM3 model (red circles) and the 0-D UWCM box model (black diamonds). Error bars denote  $3\sigma$  fitting uncertainties.

Background HCHO mixing ratios are underpredicted by 0.5–1 ppbv by both models (Fig. 4b). The range of underprediction is consistent with the offsets between observed and modeled total HCHO abundances (Fig. S5 in the Supplement fit  $x$  intercepts: 0.3 ppbv (AM3) and 1.1 ppbv (UWCM)). It is possible that both models are missing some HCHO precursors (e.g., from multi-generation isoprene oxidation or other VOC not related to isoprene). This is especially plausible for the UWCM simulation, which only includes isoprene, methane and methanol as primary VOC and does not account for horizontal transport. Underestimated OH concentrations might also explain part of this discrepancy, though we cannot easily evaluate this possibility. AM3 performs somewhat better than UWCM in terms of overall magnitude but exhibits a less clear  $\text{NO}_x$  trend, which may reflect dilution over fairly large grid scales (note that the range of binned  $\text{NO}_x$  values is smaller for AM3 than both observations and the UWCM). This result again highlights the need to consider this background before using a model to interpret observed HCHO columns that effectively average HCHO sources over space and time.

The agreement between AM3 and UWCM-MCM v3.3.1 is consistent with how these mechanisms treat first-generation ISOPO<sub>2</sub> radicals (Figs. S6 and S7 in the Supplement). Both models use the same rate constants for reactions of ISOPO<sub>2</sub>

with NO and HO<sub>2</sub>, which comprise the bulk of ISOPO<sub>2</sub> sink. The AM3 mechanism assigns a 12 % yield of HCHO to the reaction of ISOPO<sub>2</sub> with HO<sub>2</sub> (Paulot et al., 2009b), while the MCM assumes 100 % production of peroxides for this channel. This may explain some of the discrepancy in the prompt yield at low  $\text{NO}_x$  (Fig. 4a), though neither mechanism is consistent with the current experimental HCHO yield of ~6 % HCHO (Liu et al., 2013). There are also two key differences in the minor reaction channels. First, the rate constant for reaction of ISOPO<sub>2</sub> with other RO<sub>2</sub> is an order of magnitude lower in AM3 compared to MCM v3.3.1 ( $1.54$  vs.  $12\text{--}16 \times 10^{-13} \text{ cm}^3 \text{ s}^{-1}$ , the latter depending on the ISOPO<sub>2</sub> isomer distribution). This reaction produces HCHO with yields comparable to that of ISOPO<sub>2</sub> + NO and may be an important source in very low  $\text{NO}_x$  regimes. Second, AM3 assumes a constant ISOPO<sub>2</sub> isomer distribution and thus underpredicts the isomerization rate relative to MCM v3.3.1, especially at mid- to high  $\text{NO}_x$  (Fig. S7D in the Supplement). AM3 also includes HCHO and other small oxidized VOC as direct products of isomerization rather than producing hydroperoxy aldehydes and other large products, which influences the timescale of HCHO production and thus the partitioning between prompt and background HCHO. The impact of the RO<sub>2</sub> reaction and isomerization channels on HCHO yields is likely minor but depends significantly on the RO<sub>2</sub> / HO<sub>2</sub> ratio (at low  $\text{NO}_x$ ) and on the overall ISOPO<sub>2</sub> lifetime, which affects the ISOPO<sub>2</sub> isomer distribution. For the particular model conditions shown in Fig. S3B in the Supplement, ISOPO<sub>2</sub> lifetimes for the two mechanisms can differ by as much as 25 % at the lowest  $\text{NO}_x$  values (Fig. S7E). Regardless of these differences, the results shown in Fig. 4 confirm that both the condensed AM3 and explicit MCM v3.3.1 mechanisms perform similarly with regard to overall HCHO production.

## 6 Mechanistic drivers of the $\text{NO}_x$ –HCHO relationship

Despite the complexity of gas-phase organic chemistry, the impact of  $\text{NO}_x$  on HCHO production essentially reduces to two factors: radical cycling and RO<sub>2</sub> branching. Increasing NO enhances the conversion of HO<sub>2</sub> to OH (Reaction R4) and thus accelerates VOC oxidation (Reaction R5). RO<sub>2</sub> is also produced, to a lesser extent, by VOC ozonolysis and photolysis (Reaction R6). Subsequent production of HCHO depends on the structure and fate of RO<sub>2</sub> intermediates, which can react with NO, HO<sub>2</sub>, other RO<sub>2</sub>, or isomerize (Reaction R7).



Here,  $\alpha$  represents a bulk branching ratio for HCHO production weighted over all RO<sub>2</sub> reactions. The RO<sub>2</sub> lifetime is typically less than 100 s during the day, so Reaction (R5) is the rate-limiting step in HCHO formation. The HCHO production rate is then equal to the product of the total RO<sub>2</sub> production rate and the bulk branching ratio:

$$P(\text{HCHO}) = \alpha P(\text{RO}_2). \quad (3)$$

Though total RO<sub>2</sub> losses include reactions that do not make HCHO,  $\alpha$  is still a useful metric for the relationship between HCHO production and overall VOC oxidation.

To disentangle these factors, we extract chemical rates from the diel steady-state UWCM simulations discussed in Sect. 5. Figure 5a shows the gross production rates for total peroxy radicals and HCHO as a function of NO<sub>x</sub>. Consistent with our earlier discussion, HCHO production increases by a factor of 3 from low to high NO<sub>x</sub>. Total RO<sub>2</sub> production increases by a factor of 2 over this same range, driven primarily by increasing OH. The bulk branching ratio  $\alpha$ , calculated as the ratio of HCHO and RO<sub>2</sub> production rates, increases from 0.43 to 0.62 (Fig. 5b). This trend is consistent with NO<sub>x</sub>-dependent branching ratios of several major HCHO precursors, including isoprene hydroxyperoxy radicals (ISOPO<sub>2</sub>) and methyl peroxy radical (Fig. 5b). Based on this analysis, we conclude that enhanced OH production is the main driver for the NO<sub>x</sub> dependence of HCHO production, with variations in RO<sub>2</sub> branching playing a lesser (but still important) role.

Using a combination of regional modeling and satellite observations, a recent study by Valin et al. (2016) also examines the drivers of HCHO production. They concur that OH production exerts a controlling influence on HCHO throughout the southeast US. In contrast to our study, however, they assert that changes in RO<sub>2</sub> branching have a negligible effect on the HCHO–NO<sub>x</sub> dependence. There are several potential explanations for this discrepancy. First, Valin et al. (2016) derive an “effective branching ratio” that is analogous to the bulk branching ratio in Eq. (3) but calculated with reference to production of OH rather than RO<sub>2</sub>. Many OH sinks do not form RO<sub>2</sub> radicals (e.g., reaction with CO, HCHO, methanol and NO<sub>2</sub>) and thus will not make HCHO. The fractional contribution of such reactants to total modeled OH reactivity increases from 36 % to 60 % over our NO<sub>x</sub> range; thus, using P(OH) instead of P(RO<sub>2</sub>) to calculate  $\alpha$  from Eq. (3) would effectively normalize out the NO<sub>x</sub> dependence of RO<sub>2</sub> branching (Fig. 5b). Second, these two studies use very different photochemical mechanisms. Valin et al. (2016) use a modified version of the lumped Regional Atmospheric Chemistry Mechanism 2 (RACM2) (Browne et al., 2014; Goliff et al., 2013), while our box model uses the explicit MCM v3.3.1 (Jenkin et al., 2015). In Valin et al. (2016), it is stated that increasing HCHO production from the RO<sub>2</sub> + RO<sub>2</sub> channel compensates for decreasing production from RO<sub>2</sub> + NO – an effect that we do not observe.

Deeper investigation reveals that the rate constant for reaction of ISOPO<sub>2</sub> with HO<sub>2</sub> in RACM2 is a factor of 2 lower than that used in both MCM v3.3.1 and the AM3 mechanism, which is based on the experimentally derived parameterization of Boyd et al. (2003). Thus, our model predicts a significantly larger contribution of RO<sub>2</sub> + HO<sub>2</sub> (which produces negligible HCHO) to the total RO<sub>2</sub> sink. These differences highlight the importance of carefully evaluating chemical mechanisms before using models to interpret in situ and satellite observations.

Increased OH also reduces the lifetime of HCHO, which may affect the HCHO budget if this reaction becomes competitive with photolysis. UWCM predicts an average HCHO photolysis lifetime of 4 h and OH reaction lifetimes that range from 3 h at high NO<sub>x</sub> to 12 h at low NO<sub>x</sub>. Thus, photolysis is typically the dominant loss process and the scaling of HCHO lifetime with OH is typically weak. The net chemical tendency of HCHO (production minus loss) is positive and increasing throughout the range of model NO<sub>x</sub> conditions. Faster loss due to reaction with OH therefore only slightly dampens the enhancement in HCHO production.

## 7 Conclusions

Using SENEX aircraft observations, we have quantified the NO<sub>x</sub> dependence of the relationship between isoprene emission strength and HCHO mixing ratios. Simultaneous measurements of isoprene, MVK and MACR define a photochemical clock for isoprene oxidation, allowing separation of prompt HCHO production (which retains the isoprene source signature) and background HCHO from late-generation isoprene oxidation products, methane and other long-lived VOC. The prompt HCHO yield increases by a factor of 3 (0.3 to 0.9 ppbv ppbv<sup>-1</sup>) and the average background HCHO mixing ratio doubles (1.6 to 3.3 ppbv) over the range of NO<sub>x</sub> values encountered in the southeast US (0.1–2 ppbv). This analytical method is applied to evaluate the performance of a global chemical transport model and a 0-D steady-state box model. Both models accurately reproduce the observed NO<sub>x</sub> trend of the prompt HCHO yield, indicating that both chemical mechanisms accurately capture early-stage isoprene oxidation. On the other hand, both models also underpredict background HCHO abundance by 0.5–1 ppbv, which is a significant fraction of total HCHO in some cases. This suggests insufficient build-up of isoprene-derived long-lived precursors in the models, missing VOC not related to isoprene, or insufficient OH. Box model results also provide insight into the mechanistic drivers of the observed NO<sub>x</sub> trends. Over the NO<sub>x</sub> range studied here, a 100 % increase in total RO<sub>2</sub> production and a 40 % increase in the HCHO production branching ratio give rise to a 3-fold increase in total HCHO production.

To our knowledge, there are no direct laboratory measurements of HCHO yields from low-NO<sub>x</sub> isoprene chem-

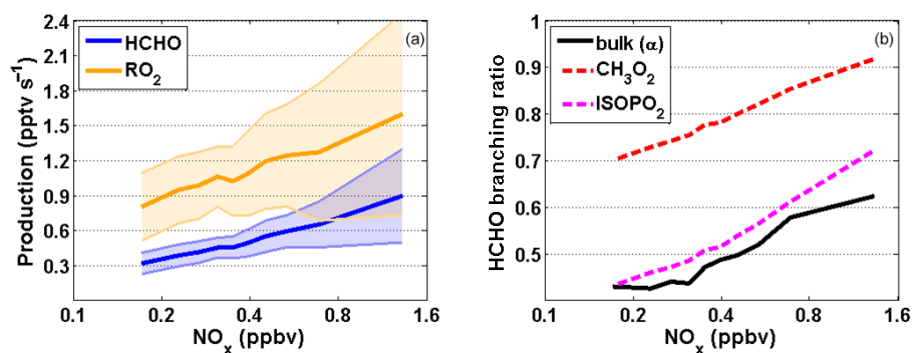


**Figure 5.**  $\text{NO}_x$  dependence of chemical properties related to HCHO production, extracted from the UWCM simulation of SENEX observations. (a) Production rates for HCHO (blue) and total  $\text{RO}_2$  (orange). (b) Branching ratios for HCHO production weighted over all  $\text{RO}_2$  (solid black line) and for several individual  $\text{RO}_2$ , including methyl peroxy radical (red) and total isoprene hydroxyperoxy radicals (magenta). All quantities are averaged over  $\text{NO}_x$  using 10 bins with equal numbers of points. In (a), solid lines show the mean and shading is  $1\sigma$  variability.

istry; thus, the results presented here constitute the first measurement-constrained evaluation of the isoprene–HCHO link across  $\text{NO}_x$  regimes. The AM3 and MCM v3.3.1 mechanisms differ substantially (the former is highly condensed, while the latter is explicit), but both contain recent updates to isoprene degradation. We expect that other mechanisms will also perform well if they accurately reflect our current best understanding. The observations presented here do not include the extremely low  $\text{NO}_x$  regime ( $\text{NO}_x < 0.1$  ppbv) typical of remote regions like the Amazon and equatorial Africa. In such pristine regions, smearing of HCHO production is expected to be more severe (Barkley et al., 2013), and total HCHO production may be significantly lower if the  $\text{RO}_2$  fate favors functionalization over fragmentation (e.g., isomerization). More work is needed to map out this area of the urban–rural spectrum. It may also be possible to apply the methods developed here to evaluate the chemistry of glyoxal, another key tracer of VOC oxidation that is also amenable to orbital observations (Kaiser et al., 2015b; Li et al., 2016) and is believed to be an important precursor for secondary organic aerosol (McNeill et al., 2012).

These results also carry implications for top-down isoprene emission estimates. Uncertainties in low- $\text{NO}_x$  chemistry are often cited as the largest source of potential error in derived emissions (Marais et al., 2012; Palmer et al., 2006). Based on our analysis, current mechanisms appear to capture low- $\text{NO}_x$  production of HCHO, MVK and MACR, thus such errors are likely less severe than commonly asserted. Recent work has acknowledged the impact of  $\text{NO}_x$  on the prompt yield of HCHO from isoprene (Marais et al., 2012). We advocate considering the  $\text{NO}_x$  dependence of background HCHO as well, since this can constitute a significant fraction of the total HCHO column. For scale, the derived background HCHO mixing ratio of 1.6–3.3 ppbv is 37–77 % of the campaign-mean observed HCHO mixing ratio of 4.3 ppbv. Forthcoming geostationary observations will resolve local gradients in chemical regime, and smearing

and background HCHO production will become problematic even in high- $\text{NO}_x$  regions. Indeed, even current-generation orbital instruments are capable of resolving some urban–rural gradients in HCHO columns (Boeke et al., 2011). When applying advanced statistical techniques like inversion, model results will only be as accurate as the chemical mechanisms driving them. Continued field observations are crucial for providing confidence in our ability to link HCHO to its sources. In this regard, recent work has highlighted the potential of airborne eddy covariance fluxes to quantify both surface–atmosphere exchange and in situ chemical processes (Karl et al., 2013; Kaser et al., 2015; Misztal et al., 2014; Wolfe et al., 2015). With such tools, it should be possible to simultaneously measure both isoprene emissions and HCHO columns, thereby obtaining a direct experimental constraint on the link between these two quantities.

#### Data availability

All data used in this study are publicly accessible on the SENEX website (<http://www.esrl.noaa.gov/csd/projects/senex/>).

**The Supplement related to this article is available online at doi:10.5194/acp-16-2597-2016-supplement.**

*Acknowledgements.* We are grateful to NOAA AOC and the flight crew of the WP-3D for enabling a super awesome mission. HCHO measurement efforts were supported by US EPA Science to Achieve Results (STAR) program grant 83540601 and NASA grant NNN10ZDA001N-SEAC4RS. Analysis was supported by NASA ACCDAM grant NNX14AP48G. J. Kaiser acknowledges support from NASA ESSF grant NNX14AK97H. C. D. Hatch was supported by the Hendrix faculty grant and the Hendrix College Odyssey program. J. Mao and L. W. Horowitz

acknowledge support from NOAA Climate Program Office grant # NA13OAR4310071. This research has not been subjected to any EPA review and therefore does not necessarily reflect the views of the agency, and no official endorsement should be inferred.

Edited by: N. L. Ng

## References

- Abbot, D. S., Palmer, P. I., Martin, R. V., Chance, K. V., Jacob, D. J., and Guenther, A.: Seasonal and interannual variability of North American isoprene emissions as determined by formaldehyde column measurements from space, *Geophys. Res. Lett.*, 30, 1886, doi:10.1029/2003GL017336, 2003.
- Atkinson, R. and Arey, J.: Gas-phase tropospheric chemistry of biogenic volatile organic compounds: a review, *Atmos. Environ.*, 37, S197–S219, 2003.
- Atkinson, R., Baulch, D., Cox, R., Crowley, J., Hampson, R., Hynes, R., Atkinson, R., Baulch, D. L., Cox, R. A., Crowley, J. N., Hampson, R. F., Hynes, R. G., Jenkin, M. E., Rossi, M. J., Troe, J., and IUPAC Subcommittee: Evaluated kinetic and photochemical data for atmospheric chemistry: Volume II – gas phase reactions of organic species, *Atmos. Chem. Phys.*, 6, 3625–4055, doi:10.5194/acp-6-3625-2006, 2006.
- Barkley, M. P., Palmer, P. I., Kuhn, U., Kesselmeier, J., Chance, K., Kurosu, T. P., Martin, R. V., Helmig, D., and Guenther, A.: Net ecosystem fluxes of isoprene over tropical South America inferred from Global Ozone Monitoring Experiment (GOME) observations of HCHO columns, *J. Geophys. Res.*, 113, D20304, doi:10.1029/2008JD009863, 2008.
- Barkley, M. P., De Smedt, I., Van Roozendaal, M., Kurosu, T. P., Chance, K., Arneth, A., Hagberg, D., Guenther, A., Paulot, F., Marais, E., and Mao, J. Q.: Top-down isoprene emissions over tropical South America inferred from SCIAMACHY and OMI formaldehyde columns, *J. Geophys. Res. Atmos.*, 118, 6849–6868, doi:10.1002/jgrd.50552, 2013.
- Boeke, N. L., Marshall, J. D., Alvarez, S., Chance, K. V., Fried, A., Kurosu, T. P., Rappengluck, B., Richter, D., Walega, J., Weibring, P., and Millet, D. B.: Formaldehyde columns from the Ozone Monitoring Instrument: Urban versus background levels and evaluation using aircraft data and a global model, *J. Geophys. Res. Atmos.*, 116, D05303, doi:10.1029/2010jd014870, 2011.
- Boyd, A. A., Flaud, P. M., Daugey, N., and Lesclaux, R.: Rate Constants for RO<sub>2</sub> + HO<sub>2</sub> Reactions Measured under a Large Excess of HO<sub>2</sub>, *J. Phys. Chem. A*, 107, 818–821, 2003.
- Brown, S. S., deGouw, J. A., Warneke, C., Ryerson, T. B., Dube, W. P., Atlas, E., Weber, R. J., Peltier, R. E., Neuman, J. A., Roberts, J. M., Swanson, A., Flocke, F., McKeen, S. A., Brioude, J., Sommariva, R., Trainer, M., Fehsenfeld, F. C., and Ravishankara, A. R.: Nocturnal isoprene oxidation over the Northeast United States in summer and its impact on reactive nitrogen partitioning and secondary organic aerosol, *Atmos. Chem. Phys.*, 9, 3027–3042, doi:10.5194/acp-9-3027-2009, 2009.
- Browne, E. C., Wooldridge, P. J., Min, K. E., and Cohen, R. C.: On the role of monoterpene chemistry in the remote continental boundary layer, *Atmos. Chem. Phys.*, 14, 1225–1238, doi:10.5194/acp-14-1225-2014, 2014.
- Carlton, A. and Baker, K.: Photochemical Modeling of the Ozark Isoprene Volcano: MEGAN, BEIS, and Their Impacts on Air Quality Predictions, *Environ. Sci. Technol.*, 45, 4438–4445, doi:10.1021/es200050x, 2011.
- Cazorla, M., Wolfe, G. M., Bailey, S. A., Swanson, A. K., Arkinson, H. L., and Hanisco, T. F.: A new airborne laser-induced fluorescence instrument for in situ detection of Formaldehyde throughout the troposphere and lower stratosphere, *Atmos. Meas. Tech.*, 8, 541–552, doi:10.5194/amt-8-541-2015, 2015.
- Crouse, J. D., Paulot, F., Kjaergaard, H. G., and Wennberg, P. O.: Peroxy radical isomerization in the oxidation of isoprene, *Phys. Chem. Chem. Phys.*, 13, 13607–13613, 2011.
- Crouse, J. D., Knap, H. C., Ørnsø, K. B., Jørgensen, S., Paulot, F., Kjaergaard, H. G., and Wennberg, P. O.: On the atmospheric fate of methacrolein: 1. Peroxy radical isomerization following addition of OH and O<sub>2</sub>, *J. Phys. Chem. A*, 116, 5756–5762, doi:10.1021/jp211560u, 2012.
- Curci, G., Palmer, P. I., Kurosu, T. P., Chance, K., and Visconti, G.: Estimating European volatile organic compound emissions using satellite observations of formaldehyde from the Ozone Monitoring Instrument, *Atmos. Chem. Phys.*, 10, 11501–11517, doi:10.5194/acp-10-11501-2010, 2010.
- da Silva, G., Graham, C., and Wang, Z. F.: Unimolecular beta-Hydroxyperoxy Radical Decomposition with OH Recycling in the Photochemical Oxidation of Isoprene, *Environ. Sci. Technol.*, 44, 250–256, 2010.
- de Gouw, J. and Warneke, C.: Measurements of volatile organic compounds in the earth's atmosphere using proton-transfer-reaction mass spectrometry, *Mass Spec. Rev.*, 26, 223–257, doi:10.1002/mas.20119, 2007.
- de Gouw, J. A., Middlebrook, A. M., Warneke, C., Goldan, P. D., Kuster, W. C., Roberts, J. M., Fehsenfeld, F. C., Worsnop, D. R., Canagaratna, M. R., Pszenny, A. A. P., Keene, W. C., Marchewka, M., Bertman, S. B., and Bates, T. S.: Budget of organic carbon in a polluted atmosphere: Results from the New England Air Quality Study in 2002, *J. Geophys. Res.*, 110, D16305, doi:10.1029/2004jd005623, 2005.
- de Gouw, J. A., McKeen, S. A., Aikin, K. C., Brock, C. A., Brown, S. S., Gilman, J. B., Graus, M., Hanisco, T., Holloway, J. S., Kaiser, J., Keutsch, F. N., Lerner, B. M., Liao, J., Markovic, M. Z., Middlebrook, A. M., Min, K. E., Neuman, J. A., Nowak, J. B., Peischl, J., Pollack, I. B., Roberts, J. M., Ryerson, T. B., Trainer, M., Veres, P. R., Warneke, C., Welti, A., and Wolfe, G. M.: Airborne Measurements of the Atmospheric Emissions from a Fuel Ethanol Refinery, *J. Geophys. Res. Atmos.*, 120, 4385–4397, doi:10.1002/2015jd023138, 2015.
- DiGangi, J. P., Boyle, E. S., Karl, T., Harley, P., Turnipseed, A., Kim, S., Cantrell, C., Maudlin Iii, R. L., Zheng, W., Flocke, F., Hall, S. R., Ullmann, K., Nakashima, Y., Paul, J. B., Wolfe, G. M., Desai, A. R., Kajii, Y., Guenther, A., and Keutsch, F. N.: First direct measurements of formaldehyde flux via eddy covariance: implications for missing in-canopy formaldehyde sources, *Atmos. Chem. Phys.*, 11, 10565–10578, doi:10.5194/acp-11-10565-2011, 2011.
- Donner, L. J., Wyman, B. L., Hemler, R. S., Horowitz, L. W., Ming, Y., Zhao, M., Golaz, J.-C., Ginoux, P., Lin, S. J., Schwarzkopf, M. D., Austin, J., Alaka, G., Cooke, W. F., Delworth, T. L., Freidenreich, S. M., Gordon, C. T., Griffies, S. M., Held, I. M., Hurlin, W. J., Klein, S. A., Knutson, T. R., Langenhorst, A. R.,

- Lee, H.-C., Lin, Y., Magi, B. I., Malyshev, S. L., Milly, P. C. D., Naik, V., Nath, M. J., Pincus, R., Ploshay, J. J., Ramaswamy, V., Seman, C. J., Shevliakova, E., Sirutis, J. J., Stern, W. F., Stouffer, R. J., Wilson, R. J., Winton, M., Wittenberg, A. T., and Zeng, F.: The Dynamical Core, Physical Parameterizations, and Basic Simulation Characteristics of the Atmospheric Component AM3 of the GFDL Global Coupled Model CM3, *J. Climate*, 24, 3484–3519, doi:10.1175/2011jcli3955.1, 2011.
- Dufour, G., Wittrock, F., Camredon, M., Beekmann, M., Richter, A., Aumont, B., and Burrows, J. P.: SCIAMACHY formaldehyde observations: constraint for isoprene emission estimates over Europe?, *Atmos. Chem. Phys.*, 9, 1647–1664, doi:10.5194/acp-9-1647-2009, 2009.
- Fares, S., Paoletti, E., Loreto, F., and Brilli, F.: Bidirectional Flux of Methyl Vinyl Ketone and Methacrolein in Trees with Different Isoprenoid Emission under Realistic Ambient Concentrations, *Environ. Sci. Technol.*, 49, 7735–7742, doi:10.1021/acs.est.5b00673, 2015.
- Fortems-Cheiney, A., Chevallier, F., Pison, I., Bousquet, P., Saunoy, M., Szopa, S., Cressot, C., Kurosu, T. P., Chance, K., and Fried, A.: The formaldehyde budget as seen by a global-scale multi-constraint and multi-species inversion system, *Atmos. Chem. Phys.*, 12, 6699–6721, doi:10.5194/acp-12-6699-2012, 2012.
- Fu, T. M., Jacob, D. J., Palmer, P. I., Chance, K., Wang, Y. X., Barletta, B., Blake, D. R., Stanton, J. C., and Pilling, M. J.: Space-based formaldehyde measurements as constraints on volatile organic compound emissions in east and south Asia and implications for ozone, *J. Geophys. Res. Atmos.*, 112, D06312, doi:10.1029/2006jd007853, 2007.
- Fuchs, H., Hofzumahaus, A., Rohrer, F., Bohn, B., Brauers, T., Dorn, H., Haseler, R., Holland, F., Kaminski, M., Li, X., Lu, K., Nehr, S., Tillmann, R., Wegener, R., and Wahner, A.: Experimental evidence for efficient hydroxyl radical regeneration in isoprene oxidation, *Nature Geosci.*, 6, 1023–1026, doi:10.1038/NNGEO1964, 2013.
- Goliff, W. S., Stockwell, W. R., and Lawson, C. V.: The regional atmospheric chemistry mechanism, version 2, *Atmos. Environ.*, 68, 174–185, doi:10.1016/j.atmosenv.2012.11.038, 2013.
- González Abad, G., Liu, X., Chance, K., Wang, H., Kurosu, T. P., and Suleiman, R.: Updated Smithsonian Astrophysical Observatory Ozone Monitoring Instrument (SAO OMI) formaldehyde retrieval, *Atmos. Meas. Tech.*, 8, 19–32, doi:10.5194/amt-8-19-2015, 2015.
- Guenther, A. B., Jiang, X., Heald, C. L., Sakulyanontvittaya, T., Duhl, T., Emmons, L. K., and Wang, X.: The Model of Emissions of Gases and Aerosols from Nature version 2.1 (MEGAN2.1): an extended and updated framework for modeling biogenic emissions, *Geosci. Mod. Dev.*, 5, 1471–1492, doi:10.5194/gmd-5-1471-2012, 2012.
- Hogrefe, C., Isukapalli, S. S., Tang, X. G., Georgopoulos, P. G., He, S., Zalewsky, E. E., Hao, W., Ku, J. Y., Key, T., and Sistla, G.: Impact of Biogenic Emission Uncertainties on the Simulated Response of Ozone and Fine Particulate Matter to Anthropogenic Emission Reductions, *J. Air Waste Man. Assoc.*, 61, 92–108, doi:10.3155/1047-3289.61.1.92, 2011.
- Jenkin, M. E., Young, J. C., and Rickard, A. R.: The MCM v3.3.1 degradation scheme for isoprene, *Atmos. Chem. Phys.*, 15, 11433–11459, doi:10.5194/acp-15-11433-2015, 2015.
- Kaiser, J., Wolfe, G. M., Bohn, B., Broch, S., Fuchs, H., Ganzeveld, L. N., Gomm, S., Haseler, R., Hofzumahaus, A., Holland, F., Jäger, J., Li, X., Lohse, I., Lu, K., Prevot, A. S. H., Rohrer, F., Wegener, R., Wolf, R., Mentel, T. F., Kiendler-Scharr, A., Wahner, A., and Keutsch, F. N.: Evidence for an unidentified non-photochemical ground-level source of formaldehyde in the Po Valley with potential implications for ozone production, *Atmos. Chem. Phys.*, 15, 1289–1298, doi:10.5194/acp-15-1289-2015, 2015a.
- Kaiser, J., Wolfe, G. M., Min, K. E., Brown, S. S., Miller, C. C., Jacob, D. J., deGouw, J. A., Graus, M., Hanisco, T. F., Holloway, J., Peischl, J., Pollack, I. B., Ryerson, T. B., Warneke, C., Washenfelder, R. A., and Keutsch, F. N.: Reassessing the ratio of glyoxal to formaldehyde as an indicator of hydrocarbon precursor speciation, *Atmos. Chem. Phys.*, 15, 7571–7583, doi:10.5194/acp-15-7571-2015, 2015b.
- Karl, T., Harley, P., Emmons, L., Thornton, B., Guenther, A., Basu, C., Turnipseed, A., and Jardine, K.: Efficient Atmospheric Cleansing of Oxidized Organic Trace Gases by Vegetation, *Science*, 330, 816–819, doi:10.1126/science.1192534, 2010.
- Karl, T., Misztal, P., Jonsson, H., Shertz, S., Goldstein, A., and Guenther, A.: Airborne Flux Measurements of BVOCs above Californian Oak Forests: Experimental Investigation of Surface and Entrainment Fluxes, OH Densities, and Damkohler Numbers, *J. Atmos. Sci.*, 70, 3277–3287, doi:10.1175/JAS-D-13-054.1, 2013.
- Kaser, L., Karl, T., Yuan, B., Mauldin III, R. L., Cantrell, C. A., Guenther, A. B., Patton, E. G., Weinheimer, A. J., Knote, C., Orlando, J., Emmons, L., Apel, E., Hornbrook, R., Shertz, S., Ullmann, K., Hall, S., Graus, M., de Gouw, J., Zhou, X., and Ye, C.: Chemistry-turbulence interactions and mesoscale variability influence the cleansing efficiency of the atmosphere, *Geophys. Res. Lett.*, 42, 10894–10903, doi:10.1002/2015GL066641, 2015.
- Kefauver, S. C., Filella, I., and Peñuelas, J.: Remote sensing of atmospheric biogenic volatile organic compounds (BVOCs) via satellite-based formaldehyde vertical column assessments, *Int. J. Remote Sens.*, 35, 7519–7542, doi:10.1080/01431161.2014.968690, 2014.
- Kim, S., Wolfe, G. M., Mauldin, L., Cantrell, C., Guenther, A., Karl, T., Turnipseed, A., Greenberg, J., Hall, S. R., Ullmann, K., Apel, E., Hornbrook, R., Kajii, Y., Nakashima, Y., Keutsch, F. N., DiGangi, J. P., Henry, S. B., Kaser, L., Schnitzhofer, R., Graus, M., Hansel, A., Zheng, W., and Flocke, F. F.: Evaluation of HO<sub>x</sub> sources and cycling using measurement-constrained model calculations in a 2-methyl-3-butene-2-ol (MBO) and monoterpene (MT) dominated ecosystem, *Atmos. Chem. Phys.*, 13, 2031–2044, doi:10.5194/acp-13-2031-2013, 2013.
- Kim, S., Kim, S. Y., Lee, M., Shim, H., Wolfe, G. M., Guenther, A. B., He, A., Hong, Y., and Han, J.: Impact of isoprene and HONO chemistry on ozone and OVOC formation in a semirural South Korean forest, *Atmos. Chem. Phys.*, 15, 4357–4371, doi:10.5194/acp-15-4357-2015, 2015.
- Knighton, W. B., Herndon, S. C., Franklin, J. F., Wood, E. C., Wormhoudt, J., Brooks, W., Fortner, E. C., and Allen, D. T.: Direct measurement of volatile organic compound emissions from industrial flares using real-time online techniques: Proton Transfer Reaction Mass Spectrometry and Tunable Infrared Laser Differential Absorption Spectroscopy, *Ind. Eng. Chem. Res.*, 51, 12674–12684, doi:10.1021/ie202695v, 2012.

- Kwok, E. S. C., Aschmann, S. M., Arey, J., and Atkinson, R.: Product formation from the reaction of the NO<sub>3</sub> radical with isoprene and rate constants for the reactions of methacrolein and methyl vinyl ketone with the NO<sub>3</sub> radical, *Int. J. Chem. Kin.*, 28, 925–934, 1996.
- Lee, M., Heikes, B. G., Jacob, D. J., Sachse, G., and Anderson, B.: Hydrogen peroxide, organic hydroperoxide, and formaldehyde as primary pollutants from biomass burning, *J. Geophys. Res. Atmos.*, 102, 1301–1309, doi:10.1029/96jd01709, 1997.
- Lerner, B. M., Gilman, J. B., Kuster, W. C., and de Gouw, J. A.: An improved, automated whole-air sampler and VOC GC-MS analysis system, in preparation, 2016.
- Li, J., Mao, J., Min, K. E., Washenfelder, R. A., Brown, S. S., Kaiser, J., Keutsch, F. N., Volkamer, R., Wolfe, G. M., Hanisco, T. F., Pollack, I. B., Ryerson, T. B., Graus, M., Gilman, J. B., Lerner, B. M., Warneke, C., de Gouw, J. A., Middlebrook, A. M., Liao, J., Welti, A., Henderson, B. H., Donner, L. J., Cooke, W. F., Paulot, F., and Horowitz, L. W.: Observational constraints on glyoxal production from isoprene oxidation and its contribution to organic aerosol over the Southeast United States, *Geophys. Res. Lett.*, in review, 2016.
- Liu, Y. J., Herdinger-Blatt, I., McKinney, K. A., and Martin, S. T.: Production of methyl vinyl ketone and methacrolein via the hydroperoxyl pathway of isoprene oxidation, *Atmos. Chem. Phys.*, 13, 5715–5730, doi:10.5194/acp-13-5715-2013, 2013.
- Luecken, D. J., Hutzell, W. T., Strum, M. L., and Pouliot, G. A.: Regional sources of atmospheric formaldehyde and acetaldehyde, and implications for atmospheric modeling, *Atmos. Environ.*, 47, 477–490, doi:10.1016/j.atmosenv.2011.10.005, 2012.
- Mao, J., Ren, X., Brune, W. H., Van Duin, D. M., Cohen, R. C., Park, J. H., Goldstein, A. H., Paulot, F., Beaver, M. R., Crouse, J. D., Wennberg, P. O., DiGangi, J. P., Henry, S. B., Keutsch, F. N., Park, C., Schade, G. W., Wolfe, G. M., and Thornton, J. A.: Insights into hydroxyl measurements and atmospheric oxidation in a California forest, *Atmos. Chem. Phys.*, 12, 8009–8020, doi:10.5194/acp-12-8009-2012, 2012.
- Mao, J., Horowitz, L. W., Naik, V., Fan, S., Liu, J., and Fiore, A. M.: Sensitivity of tropospheric oxidants to biomass burning emissions: implications for radiative forcing, *Geophys. Res. Lett.*, 40, 1241–1246, doi:10.1002/grl.50210, 2013.
- Marais, E. A., Jacob, D. J., Kurosu, T. P., Chance, K., Murphy, J. G., Reeves, C., Mills, G., Casadio, S., Millet, D. B., Barkley, M. P., Paulot, F., and Mao, J.: Isoprene emissions in Africa inferred from OMI observations of formaldehyde columns, *Atmos. Chem. Phys.*, 12, 6219–6235, doi:10.5194/acp-12-6219-2012, 2012.
- Marvin, M., Wolfe, G. M., and Salawitch, R., et al.: Evaluating mechanisms for isoprene oxidation using a constrained chemical box model and SENEX observations of formaldehyde, in preparation, 2016.
- McNeill, V. F., Woo, J. L., Kim, D. D., Schwier, A. N., Wannell, N. J., Sumner, A. J., and Barakat, J. M.: Aqueous-Phase Secondary Organic Aerosol and Organosulfate Formation in Atmospheric Aerosols: A Modeling Study, *Environ. Sci. Technol.*, 46, 8075–8081, doi:10.1021/es3002986, 2012.
- Millet, D. B., Jacob, D. J., Turquety, S., Hudman, R. C., Wu, S. L., Fried, A., Walega, J., Heikes, B. G., Blake, D. R., Singh, H. B., Anderson, B. E., and Clarke, A. D.: Formaldehyde distribution over North America: Implications for satellite retrievals of formaldehyde columns and isoprene emission, *J. Geophys. Res. Atmos.*, 111, D24S02, doi:10.1029/2005jd006853, 2006.
- Millet, D. B., Jacob, D. J., Boersma, K. F., Fu, T. M., Kurosu, T. P., Chance, K., Heald, C. L., and Guenther, A.: Spatial distribution of isoprene emissions from North America derived from formaldehyde column measurements by the OMI satellite sensor, *J. Geophys. Res. Atmos.*, 113, D02307, doi:10.1029/2007jd008950, 2008.
- Misztal, P. K., Karl, T., Weber, R., Jonsson, H. H., Guenther, A. B., and Goldstein, A. H.: Airborne flux measurements of biogenic isoprene over California, *Atmos. Chem. Phys.*, 14, 10631–10647, doi:10.5194/acp-14-10631-2014, 2014.
- Naik, V., Horowitz, L. W., Fiore, A. M., Ginoux, P., Mao, J., Aghedo, A. M., and Levy, H., II: Impact of preindustrial to present-day changes in short-lived pollutant emissions on atmospheric composition and climate forcing, *J. Geophys. Res. Atmos.*, 118, 8086–8110, doi:10.1002/jgrd.50608, 2013.
- Palmer, P. I., Jacob, D. J., Fiore, A. M., Martin, R. V., Chance, K., and Kurosu, T. P.: Mapping isoprene emissions over North America using formaldehyde column observations from space, *J. Geophys. Res. Atmos.*, 108, 4180, doi:10.1029/2002jd002153, 2003.
- Palmer, P. I., Abbot, D. S., Fu, T. M., Jacob, D. J., Chance, K., Kurosu, T. P., Guenther, A., Wiedinmyer, C., Stanton, J. C., Pilling, M. J., Pressley, S. N., Lamb, B., and Sumner, A. L.: Quantifying the seasonal and interannual variability of North American isoprene emissions using satellite observations of the formaldehyde column, *J. Geophys. Res. Atmos.*, 111, D12315, doi:10.1029/2005jd006689, 2006.
- Paulot, F., Crouse, J. D., Kjaergaard, H. G., Kroll, J. H., Seinfeld, J. H., and Wennberg, P. O.: Isoprene photooxidation: new insights into the production of acids and organic nitrates, *Atmos. Chem. Phys.*, 9, 1479–1501, doi:10.5194/acp-9-1479-2009, 2009a.
- Paulot, F., Crouse, J. D., Kjaergaard, H. G., Kurten, A., St Clair, J. M., Seinfeld, J. H., and Wennberg, P. O.: Unexpected Epoxide Formation in the Gas-Phase Photooxidation of Isoprene, *Science*, 325, 730–733, doi:10.1126/science.1172910, 2009b.
- Peeters, J. and Müller, J. F.: HO<sub>x</sub> radical regeneration in isoprene oxidation via peroxy radical isomerizations. II: experimental evidence and global impact, *Phys. Chem. Chem. Phys.*, 12, 14227–14235, doi:10.1939/c0cp00811g, 2010.
- Peeters, J., Vandenberk, S., Piessens, E., and Pultau, V.: H-atom abstraction in reactions of cyclic polyalkenes with OH, *Chemosphere*, 38, 1189–1195, 1999.
- Peeters, J., Nguyen, T. L., and Vereecken, L.: HO<sub>x</sub> radical regeneration in the oxidation of isoprene, *Phys. Chem. Chem. Phys.*, 11, 5935–5939, doi:10.1039/b908511d, 2009.
- Peeters, J., Müller, J.-F., Stavrou, T., and Nguyen, V. S.: Hydroxyl Radical Recycling in Isoprene Oxidation Driven by Hydrogen Bonding and Hydrogen Tunneling: The Upgraded LIM1 Mechanism, *J. Phys. Chem. A*, 118, 8625–8643, doi:10.1021/jp5033146, 2014.
- Pollack, I., Lerner, B., and Ryerson, T.: Evaluation of ultraviolet light-emitting diodes for detection of atmospheric NO<sub>2</sub> by photolysis - chemiluminescence, *J. Atmos. Chem.*, 65, 111–125, doi:10.1007/s10874-011-9184-3, 2010.
- Rivera-Rios, J. C., Nguyen, T. B., Crouse, J. D., Jud, W., St Clair, J. M., Mikoviny, T., Gilman, J. B., Lerner, B. M., Kaiser, J. B., de Gouw, J., Wisthaler, A., Hansel, A., Wennberg, P. O., Seinfeld, J. H., and Keutsch, F. N.: Conversion of hydroperoxides

- to carbonyls in field and laboratory instrumentation: Observational bias in diagnosing pristine versus anthropogenically controlled atmospheric chemistry, *Geophys. Res. Lett.*, 41, 8645–8651, doi:10.1002/2014gl061919, 2014.
- Roberts, J. M., Marchewka, M., Bertman, S. B., Goldan, P., Kuster, W., de Gouw, J., Warneke, C., Williams, E., Lerner, B., Murphy, P., Apel, E., and Fehsenfeld, F. C.: Analysis of the isoprene chemistry observed during the New England Air Quality Study (NEAQS) 2002 intensive experiment, *J. Geophys. Res.*, 111, D23S12, doi:10.1029/2006jd007570, 2006.
- Ryerson, T., Huey, L., Knapp, K., Neuman, J., Parrish, D., Sueper, D., and Fehsenfeld, F.: Design and initial characterization of an inlet for gas-phase NO<sub>y</sub> measurements from aircraft, *J. Geophys. Res. Atmos.*, 104, 5483–5492, doi:10.1029/1998JD100087, 1999.
- Shim, C., Wang, Y., Choi, Y., Palmer, P. I., Abbot, D. S., and Chance, K.: Constraining global isoprene emissions with Global Ozone Monitoring Experiment (GOME) formaldehyde column measurements, *J. Geophys. Res.*, 110, D24301, doi:10.1029/2004jd005629, 2005.
- Stavrakou, T., Müller, J.-F., De Smedt, I., Van Roozendaal, M., van der Werf, G. R., Giglio, L., and Guenther, A.: Evaluating the performance of pyrogenic and biogenic emission inventories against one decade of space-based formaldehyde columns, *Atmos. Chem. Phys.*, 9, 1037–1060, doi:10.5194/acp-9-1037-2009, 2009.
- Stavrakou, T., Müller, J. F., Bauwens, M., De Smedt, I., Van Roozendaal, M., Guenther, A., Wild, M., and Xia, X.: Isoprene emissions over Asia 1979–2012: impact of climate and land-use changes, *Atmos. Chem. Phys.*, 14, 4587–4605, doi:10.5194/acp-14-4587-2014, 2014.
- St. Clair, J. M., Wolfe, G. M., Rivera-Rios, J. C., Crouse, J. D., Praske, E., Kim, M. J., Thayer, M. P., Skog, K. M., Keutsch, F. N., Wennberg, P. O., and Hanisco, T. F.: Investigation of a potential HCHO measurement artifact from ISOPROOH, in preparation, 2016.
- Stroud, C., Roberts, J., Goldan, P., Kuster, W., Murphy, P., Williams, E., Hereid, D., Parrish, D., Sueper, D., Trainer, M., Fehsenfeld, F., Apel, E., Riemer, D., Wert, B., Henry, B., Fried, A., Martinez-Harder, M., Harder, H., Brune, W., Li, G., Xie, H., and Young, V.: Isoprene and its oxidation products, methacrolein and methylvinyl ketone, at an urban forested site during the 1999 Southern Oxidants Study, *J. Geophys. Res. Atmos.*, 106, 8035–8046, doi:10.1029/2000JD900628, 2001.
- Trainer, M., Williams, E., Parrish, D., Buhr, M., Allwine, E., Westberg, H., Fehsenfeld, F., and Liu, S.: Models and observations of the impact of natural hydrocarbons on rural ozone, *Nature*, 329, 705–707, doi:10.1038/329705a0, 1987.
- Valin, L. C., Fiore, A. M., Chance, K., and González Abad, G.: The role of OH production in interpreting the variability of CH<sub>2</sub>O columns in the southeast US, *J. Geophys. Res. Atmos.*, 121, 478–493, doi:10.1002/2015JD024012, 2016.
- Wagner, N. L., Brock, C. A., Angevine, W. M., Beyersdorf, A., Campuzano-Jost, P., Day, D., de Gouw, J. A., Diskin, G. S., Gordon, T. D., Graus, M. G., Holloway, J. S., Huey, G., Jimenez, J. L., Lack, D. A., Liao, J., Liu, X., Markovic, M. Z., Middlebrook, A. M., Mikoviny, T., Peischl, J., Perring, A. E., Richardson, M. S., Ryerson, T. B., Schwarz, J. P., Warneke, C., Welti, A., Wisthaler, A., Ziemba, L. D., and Murphy, D. M.: In situ vertical profiles of aerosol extinction, mass, and composition over the southeast United States during SENEX and SEAC4RS: observations of a modest aerosol enhancement aloft, *Atmos. Chem. Phys.*, 15, 7085–7102, doi:10.5194/acp-15-7085-2015, 2015.
- Warneke, C., de Gouw, J. A., Del Negro, L., Brioude, J., McKeen, S., Stark, H., Kuster, W. C., Goldan, P. D., Trainer, M., Fehsenfeld, F. C., Wiedinmyer, C., Guenther, A. B., Hansel, A., Wisthaler, A., Atlas, E., Holloway, J. S., Ryerson, T. B., Peischl, J., Huey, L. G., and Hanks, A. T. C.: Biogenic emission measurement and inventories determination of biogenic emissions in the eastern United States and Texas and comparison with biogenic emission inventories, *J. Geophys. Res. Atmos.*, 115, D00F18, doi:10.1029/2009jd012445, 2010.
- Warneke, C., Trainer, M., de Gouw, J. A., Parrish, D. D., Fahey, D. W., Ravishankara, A. R., Middlebrook, A. M., Brock, C. A., Roberts, J. M., Brown, S. S., Neuman, J. A., Lerner, B. M., Lack, D., Law, D., Huebler, G., Pollack, I., Sjostedt, S., Ryerson, T. B., Gilman, J. B., Liao, J., Holloway, J., Peischl, J., Nowak, J. B., Aikin, K., Min, K.-E., Washenfelder, R. A., Graus, M. G., Richardson, M., Markovic, M. Z., Wagner, N. L., Welti, A., Veres, P. R., Edwards, P., Schwarz, J. P., Gordon, T., Dube, W. P., McKeen, S., Brioude, J., Ahmadov, R., Bougiatioti, A., Lin, J., Nenes, A., Wolfe, G. M., Hanisco, T. F., Lee, B. H., Lopez-Hilfiker, F. D., Thornton, J. A., Keutsch, F. N., Kaiser, J., Mao, J., and Hatch, C.: Instrumentation and Measurement Strategy for the NOAA SENEX Aircraft Campaign as Part of the Southeast Atmosphere Study 2013, *Atmos. Meas. Tech. Discuss.*, doi:10.5194/amt-2015-388, in review, 2016.
- Wolfe, G. M., Crouse, J. D., Parrish, J. D., St. Clair, J. M., Beaver, M. R., Paulot, F., Yoon, T. P., Wennberg, P. O., and Keutsch, F. N.: Photolysis, OH reactivity and ozone reactivity of a proxy for isoprene-derived hydroperoxyenals (HPALDs), *Phys. Chem. Chem. Phys.*, 14, 7276–7286, doi:10.1039/c2cp40388a, 2012.
- Wolfe, G. M., Cantrell, C., Kim, S., Mauldin III, R. L., Karl, T., Harley, P., Turnipseed, A., Zheng, W., Flocke, F., Apel, E. C., Hornbrook, R. S., Hall, S. R., Ullmann, K., Henrey, S. B., DiGangi, J. P., Boyle, E. S., Kaser, L., Schnitzhofer, R., Hansel, A., Graus, M., Nakashima, Y., Kajii, Y., Guenther, A., and Keutsch, F. N.: Missing peroxy radical sources within a summertime ponderosa pine forest, *Atmos. Chem. Phys.*, 14, 4715–4732, doi:10.5194/acp-14-4715-2014, 2014.
- Wolfe, G. M., Hanisco, T. F., Arkinson, H. L., Bui, T. P., Crouse, J. D., Dean-Day, J., Goldstein, A., Guenther, A., Hall, S. R., Huey, G., Jacob, D. J., Karl, T., Kim, P. S., Liu, X., Marvin, M. R., Mikoviny, T., Misztal, P. K., Nguyen, T. B., Peischl, J., Pollack, I., Ryerson, T., St. Clair, J. M., Teng, A., Travis, K. R., Ullmann, K., Wennberg, P. O., and Wisthaler, A.: Quantifying sources and sinks of reactive gases in the lower atmosphere using airborne flux observations, *Geophys. Res. Lett.*, 42, 8231–8240, doi:10.1002/2015GL065839, 2015.
- Xu, L., Guo, H., Boyd, C. M., Klein, M., Bougiatioti, A., Cerully, K. M., Hite, J. R., Isaacman-VanWertz, G., Kreisberg, N. M., Knote, C., Olson, K., Koss, A., Goldstein, A. H., Hering, S. V., de Gouw, J., Baumann, K., Lee, S.-H., Nenes, A., Weber, R. J., and Ng, N. L.: Effects of anthropogenic emissions on aerosol formation from isoprene and monoterpenes in the southeastern United States, *P. Nat. Acad. Sci. USA*, 112, 37–42, doi:10.1073/pnas.1417609112, 2015.

Supplement of Atmos. Chem. Phys., 16, 2597–2610, 2016  
<http://www.atmos-chem-phys.net/16/2597/2016/>  
doi:10.5194/acp-16-2597-2016-supplement  
© Author(s) 2016. CC Attribution 3.0 License.



*Supplement of*

## **Formaldehyde production from isoprene oxidation across NO<sub>x</sub> regimes**

**G. M. Wolfe et al.**

*Correspondence to:* G. M. Wolfe ([glenn.m.wolfe@nasa.gov](mailto:glenn.m.wolfe@nasa.gov))

The copyright of individual parts of the supplement might differ from the CC-BY 3.0 licence.

## S1 Model Calculation of MVK, MACR and HCHO Yields

In Section 3 of the main text, we utilize model-derived first-generation yields of MVK and MACR to infer initial isoprene mixing ratios. Yields are calculated using the University of Washington Chemical Box Model (UWCMv2.2, described further in Sect. 5) driven by the Master Chemical Mechanism (MCMv3.3.1, (Jenkin et al., 2015)). The model is set up to simulate a series of pseudo-chamber experiments as follows. Meteorology is set to typical daytime surface conditions for the SENEX location and period ( $P = 1000$  mbar,  $T = 298$  K,  $RH = 75\%$ , solar zenith angle =  $10^\circ$ ). Mixing ratios of CO and O<sub>3</sub> are respectively held constant at 120 ppbv and 50 ppbv. Mixing ratios of isoprene, OH, HO<sub>2</sub> and NO<sub>2</sub> are respectively initialized at 5 ppbv, 0.04 pptv ( $2.7 \times 10^6$  cm<sup>-3</sup>), 20 pptv and  $4 \times [\text{NO}]$  and allowed to evolve in time. An additional constant HO<sub>2</sub> source, equivalent to photolysis of 5 ppbv HCHO, is also introduced to compensate for missing HO<sub>2</sub> sources that would be present under real atmospheric conditions. This modification, along with allowing OH and HO<sub>2</sub> to vary with NO<sub>x</sub>, provides better representation of the NO<sub>x</sub>-dependent fate of RO<sub>2</sub>. NO mixing ratios are held fixed at values ranging from 1 pptv to 10 ppbv. For each NO value, the model is integrated forward for one hour. First-generation yields for MVK, MACR and HCHO are calculated as the slope of the relationship between isoprene lost and product gained, i.e.  $y = \Delta[\text{product}]/\Delta[\text{isoprene}]$ . The fitting window is restricted to minutes 5 – 10 of the simulation to minimize effects of model spin-up and multi-generation chemistry. Resulting yield curves are shown in Fig. S3A. Model-derived yields of MVK and MACR are consistent with recent lab-derived yields at both high (Liu et al., 2013) and low (Fuchs et al., 2013) NO<sub>x</sub>. Within the range of NO mixing ratios observed during SENEX, simulated OH, HO<sub>2</sub> and RO<sub>2</sub> values (Fig. S3B) are comparable to those calculated in the full 0-D steady-state simulation (Sect. 5) and we have good confidence in the accuracy of calculated yields. Outside of this range ( $< 20$  pptv NO), calculated yields are less certain due to a lack of constraints on model HO<sub>2</sub> and RO<sub>2</sub> concentrations. At the very-low NO<sub>x</sub> end, 30 – 40% of the carbonyl yield stems from isoprene ozonolysis (thin lines in Fig. S3A), with the remainder resulting from a combination of ISOPO<sub>2</sub> + RO<sub>2</sub> and ISOPO<sub>2</sub> 1,5-H-shift isomerization channels.

## References

Fuchs, H., Hofzumahaus, A., Rohrer, F., Bohn, B., Brauers, T., Dorn, H., Haseler, R., Holland, F., Kaminski, M., Li, X., Lu, K., Nehr, S., Tillmann, R., Wegener, R., and Wahner, A.: Experimental evidence for efficient hydroxyl radical regeneration in isoprene oxidation, *Nature Geosci.*, 6, 1023-1026, doi: 10.1038/NGEO1964, 2013.

Jenkin, M. E., Young, J. C., and Rickard, A. R.: The MCM v3.3.1 degradation scheme for isoprene, *Atmos. Chem. Phys.*, 15, 11433-11459, doi: 10.5194/acp-15-11433-2015, 2015.

Liu, Y. J., Herdinger-Blatt, I., McKinney, K. A., and Martin, S. T.: Production of methyl vinyl ketone and methacrolein via the hydroperoxyl pathway of isoprene oxidation, *Atmos. Chem. Phys.*, 13, 5715-5730, doi: 10.5194/acp-13-5715-2013, 2013.

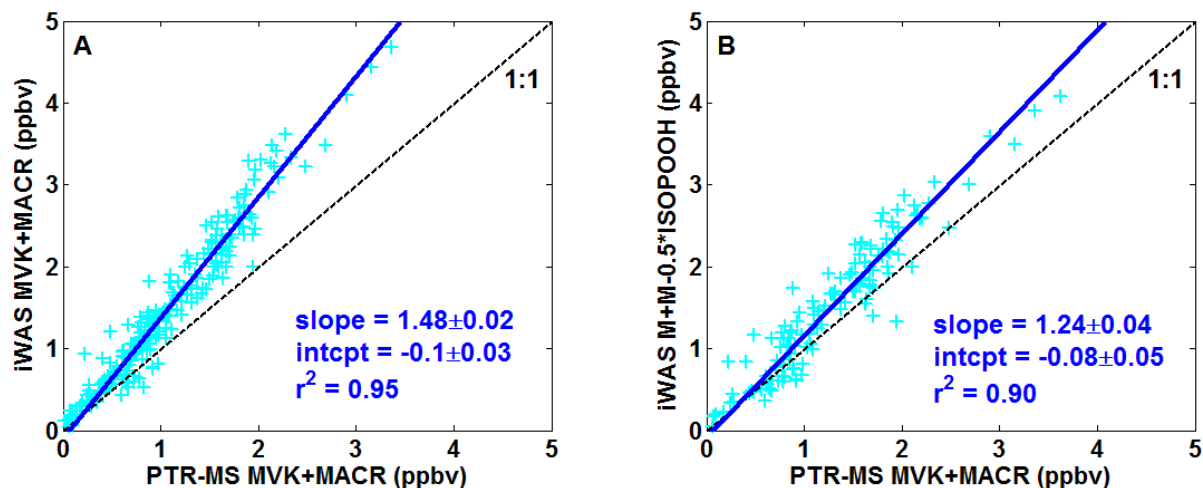


**Figure S1.** (A) Comparison of PTR-MS and iWAS observations of the sum of MVK+MACR. PTR-MS observations are averaged over the iWAS sampling start and stop times. Dashed line shows the 1:1 correlation axis, and solid blue line and text is a major axis least-squares fit that minimizes residuals in both dimensions. Quoted fitting uncertainties are  $1\sigma$ . (B) same as (A) but with a correction to iWAS assuming a 50% conversion efficiency of ISOPOOH (see Fig. S2).

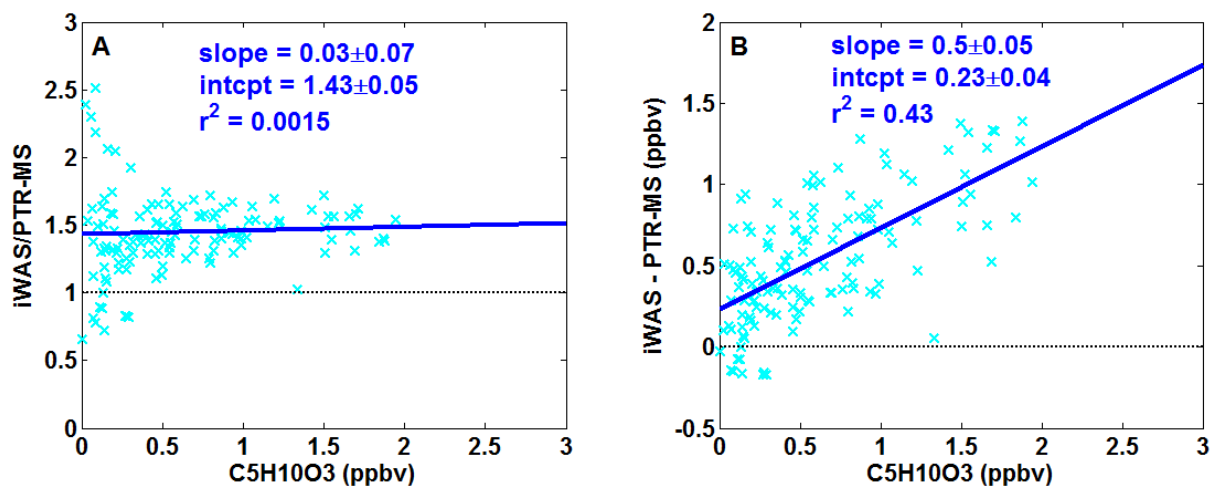


**Figure S2.** Correspondence between ISOPOOH mixing ratios (nominally  $C_5H_{10}O_3$ ) and the ratio (A) or difference (B) of iWAS and PTR-MS measurements of MVK+MACR. Solid blue lines and text represent simple least-squares fits with their  $1\sigma$  uncertainty. Dotted lines are guides for the eye.

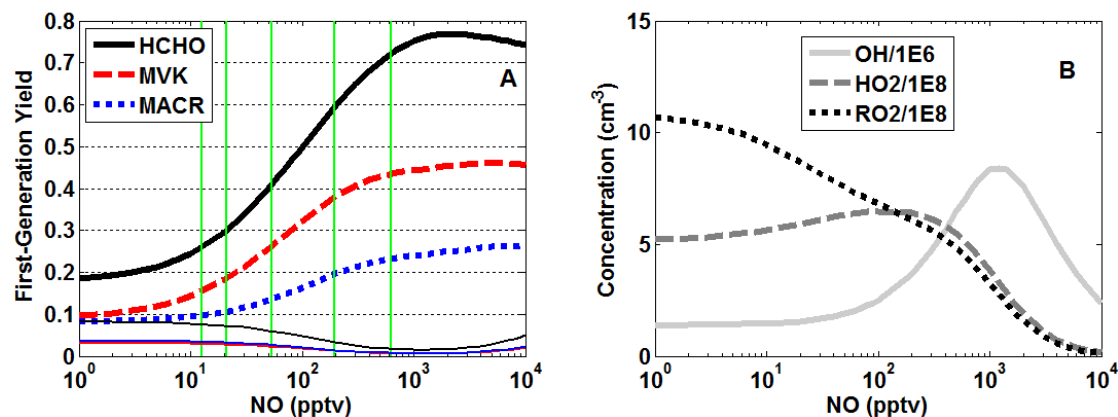


**Figure S3.** (A) NO dependence of the first-generation yields of HCHO, MVK and MACR from isoprene oxidation. Yields are derived from box model calculations using MCMv3.3.1 chemistry as described in the SI text. Thin green vertical lines denote, from left to right, the 1<sup>st</sup>, 5<sup>th</sup>, 50<sup>th</sup>, 95<sup>th</sup> and 99<sup>th</sup> percentiles of daytime boundary layer NO observed during SENEX. Thin solid lines represent the fractional yield from isoprene ozonolysis. (B) Model-calculated concentrations of OH, HO<sub>2</sub> and total RO<sub>2</sub> for the yield simulations. Concentrations are averaged over the 300 – 600 s yield fitting window for each NO value. The minimum OH concentration is  $\sim 1.4 \times 10^6 \text{ cm}^{-3}$ .

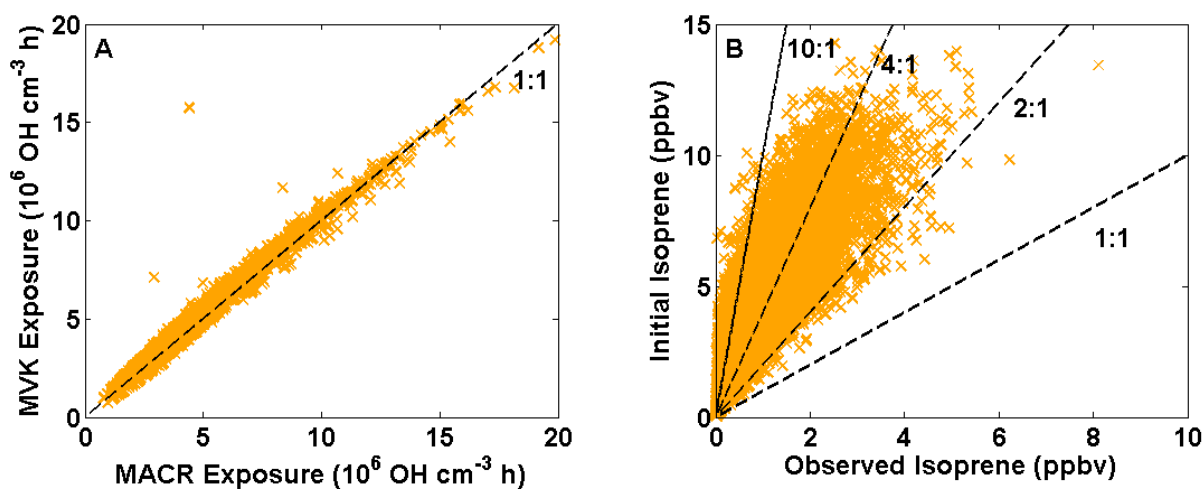


**Figure S4.** (A) Photochemical exposures (product of OH concentration and reaction time) derived from PTR-MS observations of the sum and MVK and MACR as described in Sect. 3 of the main text. PTR-MS measurements are partitioned into MVK and MACR using the MVK/MACR ratio derived from a 0-D box model simulation. The dashed line denotes a 1:1 relationship. (B) Comparison of observed and initial isoprene mixing ratios. Dashed lines denote slopes for different ratios of initial to observed isoprene.

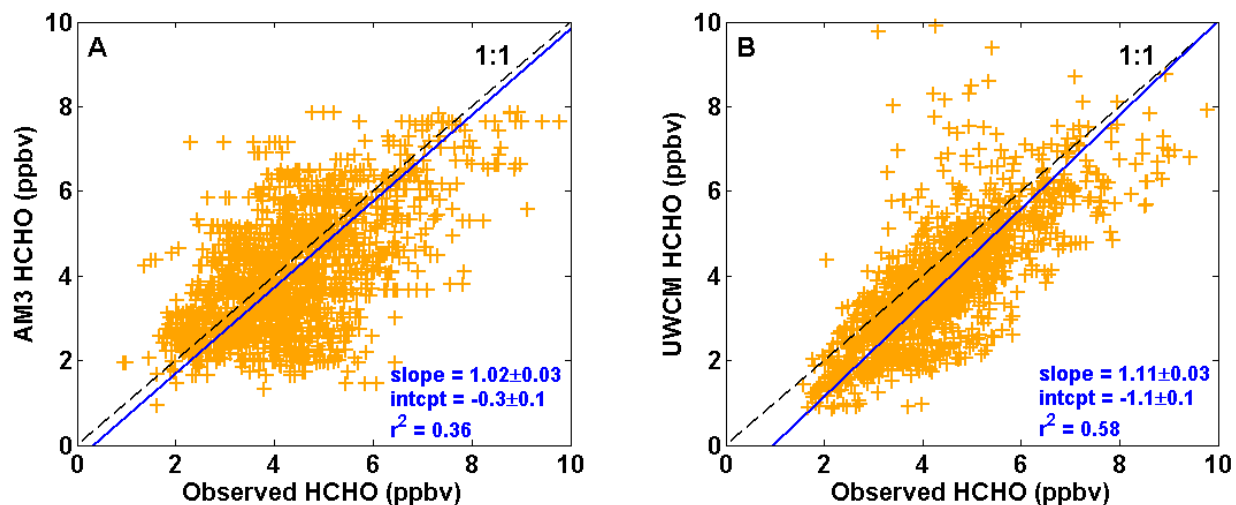


**Figure S5.** Comparison of observed and modeled HCHO mixing ratios for (A) the AM3 global chemical transport model and (B) the UWCM 0-D box model. Observations and model results are averaged/simulated at 1-minute resolution and filtered to only include daytime, boundary layer, non-biomass burning regions. Dashed lines represent the 1:1 correlation, and solid blue lines represent major axis least-squares fits. Corresponding slopes, intercepts and coefficients of determination ( $r^2$ ) are also shown with their  $1\sigma$  fitting uncertainty.

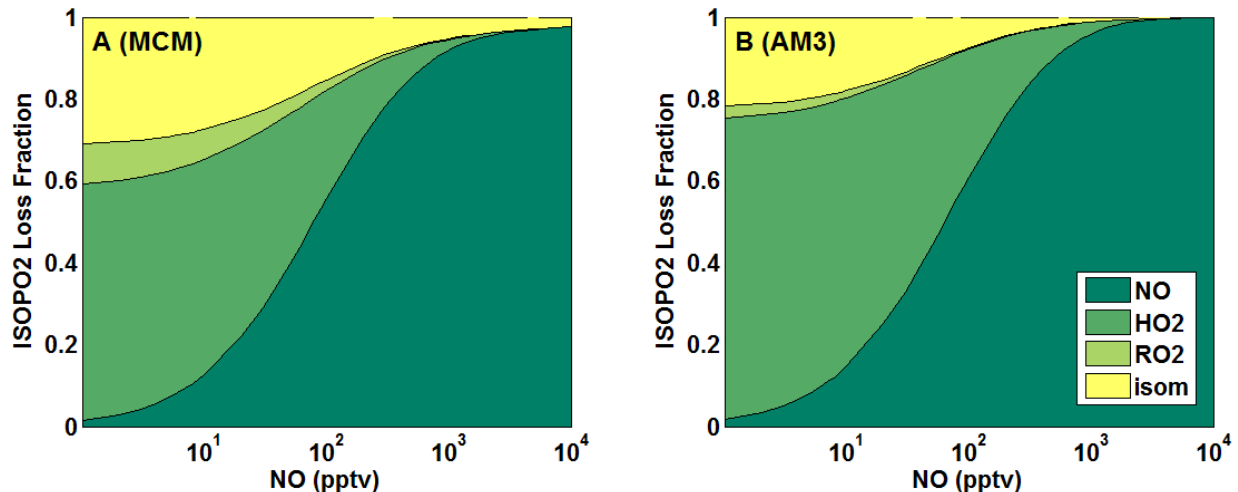


**Figure S6.** Fractional contributions of NO, HO<sub>2</sub>, RO<sub>2</sub> and isomerization to total ISOPO<sub>2</sub> loss as a function of NO. Loss fractions for MCMv3.3.1 (A) are calculated by extracting instantaneous rates for all 7 ISOPO<sub>2</sub> isomers from the yield simulations described in Section S1 and averaging these over the same timeframe used to calculate yields (300 – 600 s). Loss fractions for AM3 (B) are calculated using the NO, HO<sub>2</sub> and RO<sub>2</sub> mixing ratios from the same simulation (Fig. S3B) and rate constants provided on the GEOS-chem wiki ([http://wiki.seas.harvard.edu/geos-chem/index.php/New\\_isoprene\\_scheme](http://wiki.seas.harvard.edu/geos-chem/index.php/New_isoprene_scheme), last accessed 20 January 2016).

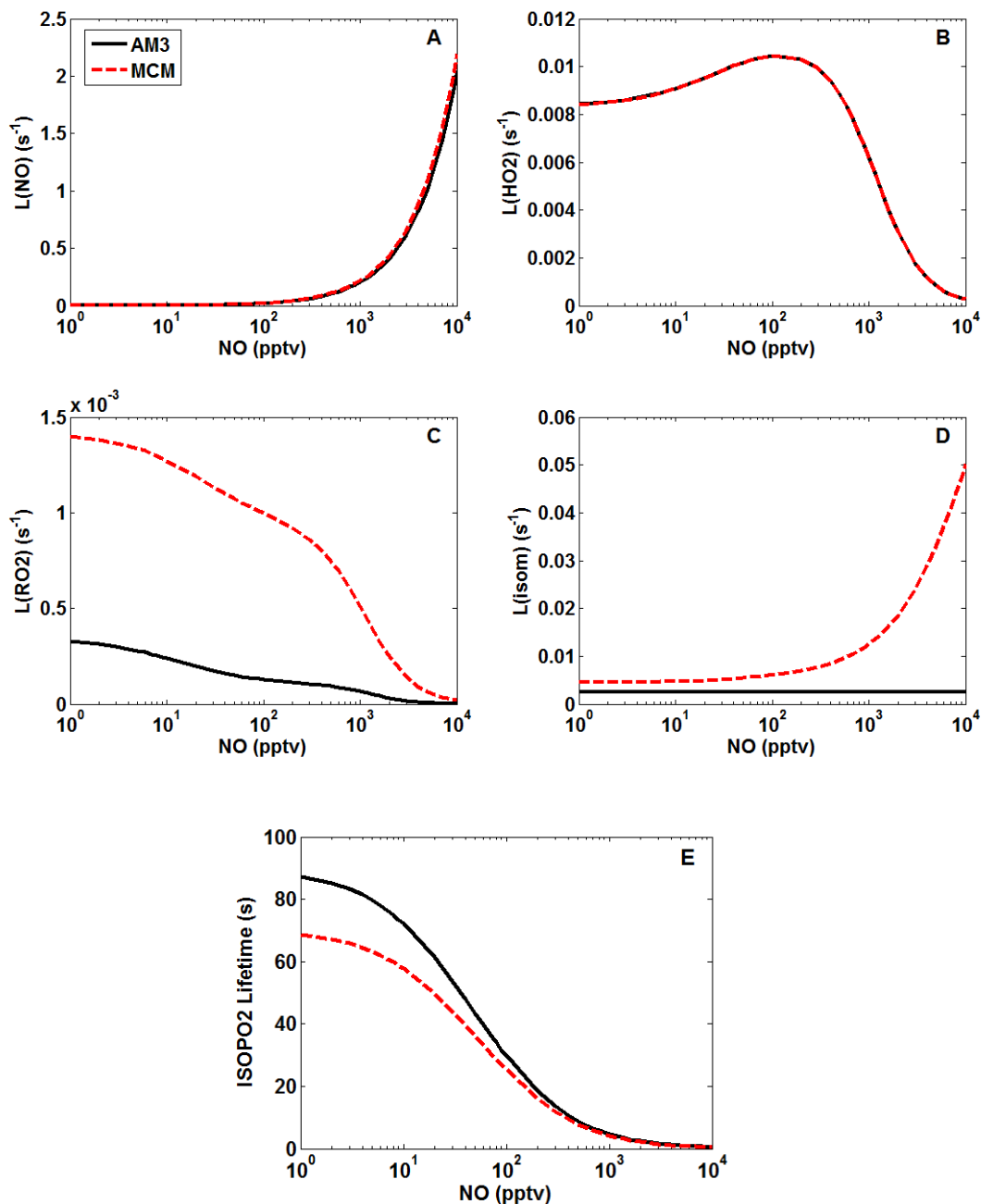


**Figure S7.** Comparison of absolute ISOPO<sub>2</sub> reactivities for the AM3 (black solid line) and MCMv3.3.1 (red dashed line) chemical mechanisms against reaction with NO (A), HO<sub>2</sub> (B), RO<sub>2</sub> (C) and isomerization (D). Reactivities are calculated using the methods described in the Fig. S6 caption. Also shown is the total ISOPO<sub>2</sub> lifetime (E).